

RECHARGE BENEATH LOW IMPACT DEVELOPMENT AND THE
EFFECTS OF CLIMATE VARIABILITY

AS
36
2012
GEOL
.N49

A thesis submitted to the faculty of
San Francisco State University
In partial fulfillment of
The requirement for
The degree

Master of Science
In
Geosciences

by

Michelle E. Newcomer

San Francisco, California

May 2012

CERTIFICATION OF APPROVAL

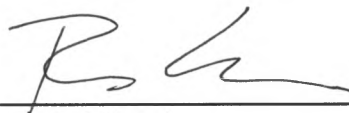
I certify that I have read Recharge Beneath Low Impact Development and the Effects of Climate Variability by Michelle E. Newcomer, and that in my opinion this work meets the criteria for approving a thesis submitted in partial fulfillment of the requirements for the degree: Master of Science in Geosciences at San Francisco State University.



Jason J. Gurdak
Professor of Geoscience



Leonard Sklar
Professor of Geoscience



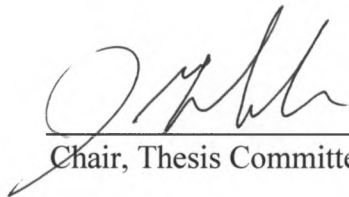
Rachel Kraai
San Francisco Public Utilities Commission

RECHARGE BENEATH LOW IMPACT DEVELOPMENT AND THE
EFFECTS OF CLIMATE VARIABILITY

Michelle E. Newcomer
San Francisco State University
2012

Groundwater resources in urban, coastal environments are highly vulnerable to human pressures and climate variability. Impervious surfaces often overflow sewage systems, prevent infiltration, and reduce recharge to aquifers. To mitigate these effects, cities worldwide are adopting Low Impact Development (LID) approaches that are hypothesized to increase infiltration and recharge rates to aquifers. The effects of LID on recharge rates are unknown, particularly in response to interannual variability of the El Niño Southern Oscillation (ENSO). Results from this study indicate recharge rates are enhanced by one order of magnitude beneath LID compared with an irrigated grass lawn and are greater during El Niño years. Recharge rates are projected to increase by 100 mm/year beneath LID and increase 6.9% under forecasted El Niño years as compared to current El Niño years. This work highlights the benefits of LID to capture and store stormwater during El Niño years, which can help urban planners manage above average water volumes introduced from climate variability.

I certify that the Abstract is a correct representation of the content of this thesis.



Chair, Thesis Committee

5-10-2012

Date

ACKNOWLEDGMENTS

I would like to acknowledge the support from the G.A. Harris Research Instrumentation Grant from Decagon Devices for providing the equipment necessary to conduct this project. I also would like to thank the Geological Society of America for the research grant providing the funding for the Hydrus-3D purchase. Additionally I would like to gratefully extend my thanks to the many people in my life who helped me through this research process including my thesis advisors, Jason Gurdak, Leonard Sklar, and Rachel Kraai, and my friends and family. I would also like to acknowledge the efforts of Joshua Benton who helped me derive the Richards Equation and helped me understand the fundamental mathematics inherent in this project. Additionally I would like to acknowledge San Francisco State University students Ryan Corbett, Ryan Ford, Mays Danfoura, Gaby Geyer, Elzie Velasco, Zip Akyurek, Elizabeth Peters, Carrie Thomas who helped with the data collection at my study sites.

TABLE OF CONTENTS

LIST OF TABLES	vi
LIST OF FIGURES	vii
1.0 Chapter 1—Introduction	1
1.1 Overview	1
1.2 Background and Problem Statement	1
1.3 Low Impact Development and Integrated Management Practices	3
1.4 Objectives and Hypotheses.....	6
1.5 References	8
2.0 Chapter 2—Recharge Beneath Low Impact Development	12
3.0 Introduction	13
4.0 Study Area Description	18
5.0 Methods.....	20
5.1 Vadose Zone Data Collection.....	20
5.2 Climate Variability	22
5.3 Stormwater Capture Capacity.....	26
5.4 Recharge	30
6.0 Results and Discussion.....	37
6.1 Time series of water content and matric potential.....	37
6.2 Historical Precipitation.....	38
6.3 Future Precipitation Scenarios.....	39
6.4 Stormwater Capture Efficiency	40
6.5 Runoff.....	42
6.6 Recharge	43
7.0 Conclusions	46
8.0 Acknowledgments.....	48
9.0 References	49
10.0 Figures and Tables.....	59
11.0 Chapter 3—Supporting Information.....	78

11.1	Experimental Field Set-up	78
11.2	LID Stormwater Capture Capacity	80
11.3	Methods for estimating recharge	83
11.4	Darcy Method	86
11.5	Water Budget Method.....	87
11.6	Recharge Probability.....	88
11.7	Modeling Recharge	94
11.8	Laboratory Analysis.....	97
11.9	RETC	97
11.10	References.....	99

LIST OF TABLES

Table 1: Rain depths associated with different probability return intervals.	72
Table 2: van Genuchten parameters for the irrigated turf grass lawn.....	72
Table 3: van Genuchten parameters for the LID infiltration trench.	72
Table 4: Summary statistics for hourly and daily data from the Mission Dolores station, SF.	73
Table 5: Daily percent change averaged by month under the GFDL A1F1 scenario.	74
Table 6: Daily intensity percent change under the GFDL A1F1 scenario.....	74
Table 7: Recharge calculated for the 2011-2012 water year for the infiltration trench and grass lawn.....	75
Table 8: Recharge calculated from the probability analysis for the different precipitation scenarios in the infiltration trench.	76
Table 9: Recharge calculated from the probability analysis for the seven different historical and predicted precipitation scenarios in the grass lawn.....	77

LIST OF FIGURES

Figure 1: The Westside Basin aquifer located on the San Francisco Peninsula, CA. The infiltration trench is shown in the top right photo and the grass lawn in the lower right. Map credit to [<i>HydroFocus Inc.</i> , 2012].....	59
Figure 2: Instrumentation setup for the infiltration trench (top) and the irrigated grass lawn (bottom). Green dots show the locations of the water content and matric potential sensors throughout the soil column.	60
Figure 3: Historical monthly precipitation distribution for the study site.	61
Figure 4: Modeled historical GFDL20th century and forecasted GFDL 21st century future daily precipitation probability densities.	62
Figure 5: Hydrus-2D model domain for the irrigated grass lawn (left) and the infiltration trench (right). Pressure heads (L) associated with each color are shown in the figure legends.....	63
Figure 6: Infiltration trench total potential profiles.	64
Figure 7: Infiltration trench water content during the summer and fall 2011, and spring 2012.....	65
Figure 8: Infiltration trench total potentials during the summer and fall 2011.....	66
Figure 9: Trench storage capacity during the largest recorded storm. Over 140 mm of precipitation occurred in just one day and over 170 mm over 2 days.....	67
Figure 10: Percent of water capture and stored by the gravel in the infiltration trench is shown and is separated by the magnitude of the rain event.	68
Figure 11: Probability distributions of yearly historical and future precipitation events and the associated runoff probability distributions from the precipitation probabilities.....	69
Figure 12: Cumulative flux at the free-drainage boundary of the Hydrus-2D model domain.....	70
Figure 13: Water budget for the infiltration trench (top) and the grass lawn (bottom).....	71

Figure 14: Maximum drainage area for the LID infiltration pond.....	79
Figure 15: Cross-section of the infiltration trench and the three piezometers with pressure transducers	79
Figure 16: Infiltration rates and cumulative infiltration for the LID infiltration pond under different water input scenarios.....	82
Figure 17: Location of the cups used for the irrigation audit.	88
Figure 18: Exponential probability density function for the historical precipitation data.	91
Figure 19: Exceedence probability of 2, 5, 10, 25, and 50 year 1-hr, 6-hr, and 24-hr storms. ENSO events are shown in blue and red.....	94
Figure 20: Water retention curves for the 4 soil samples taken at the infiltration LID site.	99

1.0 Chapter 1—Introduction

1.1 Overview

The thesis document is organized as follows. Chapter 1 provides the context of the research, including background and problem statement and overview of low impact development (LID) and best management practices (BMPs). Research hypotheses and objectives are also listed in Chapter 1. Chapter 2 is the main body of the thesis and is formatted as a manuscript that will be submitted to the peer-reviewed journal *Water Resources Research*. The research presented in Chapter 2 quantifies recharge beneath an LID infiltration trench and irrigated lawn under historical and future climate variability that is influenced by the El Niño Southern Oscillation (ENSO). Chapter 3 is the supporting information that is not appropriate for a peer-reviewed journal article, and includes additional background information about the methods and ancillary analysis presented in Chapter 2.

1.2 Background and Problem Statement

Coastal regions support approximately one-quarter of the global population, but contain less than 10% of the global-renewable water supply and are undergoing rapid population growth [*Kundzewicz et al.*, 2007]. Groundwater resources in urban, coastal environments are highly vulnerable to increased

human pressures, climate variability and change [Treidel *et al.*, 2012]. In the United States between 1950 and 2005, the population doubled and experienced a major shift from rural to urban areas, increasing the pressures on urban groundwater resources [Kenny *et al.*, 2009]. Similarly in California, groundwater depletion threatens the water supply for the State's multibillion dollar agricultural economy and drinking needs for its growing population centers, which are largely located on the California Coastal aquifer system [Maupin and Barber, 2005; Kenny *et al.*, 2009]. Coastal aquifers, such as those in California are increasingly vulnerable to seawater intrusion because of human demand and rising sea levels from climate variability and change [Treidel *et al.*, 2012].

Impervious surfaces in urban areas, such as buildings, roads, and parking lots prevent infiltration, increase contaminants in surface runoff that often overflow sewage systems, and reduce recharge to underlying aquifers. To mitigate these effects, cities worldwide are adopting low impact development (LID) site planning and best management practices (BMPs). LID BMP features are microscale and distributed management techniques that include bio-swales, rain-gardens, and infiltration trenches [Department of Environmental Resources, 1999], which reduce, filter, and slow stormwater runoff, and are hypothesized to increase infiltration and recharge rates to aquifers [SFPUC, 2010]. However, the effects of LIDs on recharge rates is not well documented, particularly during

intense precipitation events, such as those caused by interannual variability of the El Niño/Southern Oscillation (ENSO).

ENSO climate variability is a source of natural precipitation change for many regions around the Pacific Rim. ENSO is an important temporal control on the timing and magnitude of precipitation, drought, runoff and streamflow, and generally results in increased precipitation for regions such as California [Miller, 2003]. Some studies indicate that ENSO can enhance or reduce recharge rates to groundwater depending on the phase of the ENSO cycle [Gurdak *et al.*, 2007, 2009; Holman *et al.*, 2009, 2011; Tremblay *et al.*, 2011]. During the El Niño phase of ENSO that results in positive precipitation anomalies for much of California, LID features may capture more excess water that would otherwise runoff into the stormwater system and enhance more recharge to underlying aquifers as compared to naturally vegetated or irrigated areas. The excess stormwater that was captured and recharged to the underlying aquifer during wet years may provide an additional source of water during the subsequent dry years that are associated with the La Niña phase of ENSO.

1.3 Low Impact Development and Integrated Management Practices

LID and BMPs are increasingly being used in cities worldwide to mitigate the effects of urbanization on combined and separate storm-sewer systems, and increase recharge to urban aquifers [SFPUC and Wastewater Enterprise, 2009].

Water quantity is an important consideration for urban water management practices. Reduction in peak flow to stormwater systems can provide a vital service to overburdened systems. A number of studies have characterized the reduction in outflow in the storm-sewer system as a way of measuring the effectiveness of the BMPs [Davis, 2008; Schlea, 2011]. In a review of ten different studies analyzing inflow from runoff and outflow in the storm-sewer system, Schlea [2011] cites the runoff reduction as ranging typically between 40-90%. Davis [2008] monitored runoff inflows and storm-sewer outflows for two bioretention facilities showing reduction in runoff of 49 and 58% for the two devices. In 15% of the BMPs monitored by Davis [2008], 100% of the inflow water was captured by the BMP and retained without any outflow to the storm-sewer system, while the other 85% filled the BMP to capacity and caused outflow to the storm-sewer system. This is consistent with their conclusion that the BMPs have a 20% probability for volume exceedence based on the size of the system and the discharge volumes associated with each rain event.

While runoff reduction of BMPs and the recharge quality have been well characterized [Davis, 2008; Dietz and Clausen, 2005, 2006, 2008; Schlea, 2011], the rate and quantity of recharge beneath BMPs has not been well studied or quantified [Davis et al., 2009; Roy-Poirier et al., 2010]. Some municipalities have investigated urban stormwater capture for groundwater recharge on a large scale through the use of yearly water budgets, groundwater flow models, and

infiltration rates for cost-benefit analysis [*Nightingale, 1975; Dewoody et al., 2006*]. These studies have not measured in-situ groundwater recharge and do not address microscale recharge as a function of climate variability or the benefit of LID compared with the lower-cost alternative of a naturally vegetated site.

The potential recharge volume beneath an BMP is likely a function of the runoff draining into the feature, precipitation intensity that affects runoff, and the time varying storage capacity. In a review of the LID literature, *Dietz [2007]* cites two BMPs that had a >90% retention rate of precipitation falling on the impervious surface, and highlights the importance of monitoring for stormwater capture and recharge. Another study found that approximately 80% of precipitation and subsequent runoff was captured by an infiltration swale [*Ermilio and Traver, 2006*]. Based on groundwater mounding and modeling estimates, *Stephens et al. [2012]* reported recharge rates beneath BMPs ranging from 0.076-0.190 to 1.0 m/year, respectively, and concluded that approximately 50% of precipitation on a housing development in semiarid/arid New Mexico becomes recharge.

Quantifying recharge beneath BMPs would have direct benefit in States such as New Jersey where the Department of Environmental Protection Stormwater Management Rules N.J.A.C. 7:8 require that the post-development annual recharge must match that of pre-development conditions. Such requirements involve estimating pre- and post-development recharge volumes and

the annual recharge volume beneath BMPs [NJDEP New Jersey Department of Environmental Protection, 2004].

As the population and water demands increase, conservation and LID will become an increasingly important management tool. The planned use of BMPs to enhance recharge has the potential to be a valuable adaptation approach to lower the vulnerability of urban, coastal groundwater resources to the coupled effects of human pressures, climate variability and change. Existing BMPs installed with the primary objectives of reducing flooding and the impacts on overburdened stormwater systems may also have the secondary benefit of enhancing recharge and mitigating seawater intrusion in coastal aquifers. Improving understanding on the spatial, temporal, and subsurface controls on recharge beneath BMPs has important implications for water resource management, particularly for communities installing new BMPs for stormwater and (or) recharge benefits.

1.4 Objectives and Hypotheses

The primary objective of this study is to quantify, compare, and characterize controlling factors of urban recharge rates beneath a recently installed (2009) LID infiltration trench and an irrigated urban grass-lawn site. I hypothesize that the LID feature, as a site of focused recharge, has a comparatively larger surface area available for ponding that will result in greater water contents, total potential gradients that increase monotonically with depth

below land surface, more pronounced infiltration profiles from large influxes of runoff, and substantially greater recharge rates. Conversely, I hypothesize that the irrigated grass-lawn site represents a zone of diffuse recharge, and while infiltration may occur, evapotranspiration may limit deeper percolation and recharge rates as compared to the BMP.

The second objective was to simulate historical and future ENSO high-rain scenarios to evaluate the effectiveness of LID in capturing runoff and enhancing recharge in response to climate variability. I hypothesize that recharge rates will be greater beneath the BMP compared with the irrigated grass lawn during any given year because of large runoff volumes entering the system. I hypothesize that increased recharge rates beneath the diffuse and focused recharge sites are statistically correlated to El Niño winter precipitation. Intense winter precipitation from El Niño will likely translate into greater recharge at the focused BMP site compared with the diffuse (irrigated grass lawn) site because of enhanced runoff from the surrounding impervious areas into the BMP. Testing these hypotheses will help to answer many questions regarding the effect of ENSO on infiltration and recharge and how these relations may change under future precipitation scenarios.

Practical questions and implications of this research are of concern to local stormwater managers, and results from this study can translate beyond the city limits to other urban areas implementing LID. This work addresses the

stormwater capture effectiveness of the LID infiltration trench for storms of different magnitudes to evaluate how well the infiltration trench is performing relative to expectations. This research also provides recommendations to urban stormwater managers on design guidelines for the infiltration trench and provides a practical analysis regarding the numerous recharge methods that could be employed.

1.5 References

- Davis, A. P. (2008), Field performance of bioretention: Hydrology impacts, *Journal of Hydrologic Engineering*, 13, 90.
- Davis, A. P., W. F. Hunt, R. G. Traver, and M. Clar (2009), Bioretention Technology: Overview of Current Practice and Future Needs, *Journal of Environmental Engineering*, 135(3), 109–117, doi:10.1061/(ASCE)0733-9372(2009)135:3(109).
- Department of Environmental Resources (1999), *Low-Impact Development Hydrologic Analysis*, Department of Environmental Resources, Programs and Planning Division, Prince George's County, Maryland. [online] Available from:
http://www.lowimpactdevelopment.org/pubs/LID_Hydrology_National_Manual.pdf (Accessed 2 September 2011)
- Dewoody, A., W. B. Cutter, and D. Crohn (2006), Costa and Infiltration Benefits of the Watershed Augmentation Study Sites, [online] Available from:
http://www.lasgrwc.org/WAS/Documents/UCR_LASGRWC_041806.pdf
- Dietz, M. E. (2007), Low Impact Development Practices: A Review of Current Research and Recommendations for Future Directions, *Water, Air, and Soil Pollution*, 186(1-4), 351–363, doi:10.1007/s11270-007-9484-z.

- Dietz, M. E., and J. C. Clausen (2005), A Field Evaluation of Rain Garden Flow and Pollutant Treatment, *Water, Air, and Soil Pollution*, 167(1-4), 123–138, doi:10.1007/s11270-005-8266-8.
- Dietz, M. E., and J. C. Clausen (2006), Saturation to Improve Pollutant Retention in a Rain Garden, *Environmental Science & Technology*, 40(4), 1335–1340, doi:10.1021/es051644f.
- Dietz, M. E., and J. C. Clausen (2008), Stormwater runoff and export changes with development in a traditional and low impact subdivision, *Journal of Environmental Management*, 87(4), 560–566, doi:16/j.jenvman.2007.03.026.
- Ermilio, J. R., and R. G. Traver (2006), Hydrologic and Pollutant Removal Performance of a Bio-Infiltration BMP, in *Proceedings of the World Environmental and Water Resources Congress*, vol. 200, pp. 394–394, ASCE. [online] Available from: <http://link.aip.org/link/ASCECP/v200/i40856/p394/s1&Agg=doi> (Accessed 25 March 2012)
- Gurdak, J. J., R. T. Hanson, P. B. McMahon, B. W. Bruce, J. E. McCray, G. D. Thyne, and R. C. Reedy (2007), Climate Variability Controls on Unsaturated Water and Chemical Movement, High Plains Aquifer, USA, *Vadose Zone Journal*, 6(3), 533–547, doi:10.2136/vzj2006.0087.
- Gurdak, J. J., R. T. Hanson, and T. R. Green (2009), *Effects of Climate Variability and Change on Groundwater Resources of the United States*, Effects of Climate Variability and Change on Groundwater Resources of the United States: U.S. Geological Survey Fact Sheet 2009-3074. [online] Available from: <http://pubs.usgs.gov/fs/2009/3074/> (Accessed 6 March 2012)
- Holman, I. P., M. Rivas-Casado, N. J. K. Howden, J. P. Bloomfield, and A. T. Williams (2009), Linking North Atlantic ocean - atmosphere teleconnection patterns and hydrogeological responses in temperate groundwater systems, *Hydrol. Process.*, 23, 2123–2126.
- Holman, I. P., M. Rivas-Casado, J. P. Bloomfield, and J. J. Gurdak (2011), Identifying non-stationary groundwater level response to North Atlantic ocean-atmosphere teleconnection patterns using wavelet coherence, *Hydrogeol. J.*, 19(6), 1269–1278, doi:10.1007/s10040-011-0755-9.

- Kenny, J. F., N. L. Barber, S. S. Hutson, K. S. Linsey, J. K. Lovelace, and M. A. Maupin (2009), *Estimated Use of Water in the United States in 2005*, U.S. Geological Survey. [online] Available from: <http://pubs.usgs.gov/circ/1344/pdf/c1344.pdf> (Accessed 10 April 2010)
- Kundzewicz, Z. W., L. J. Mata, N. W. Arnell, P. Doll, P. Kabat, B. Jimenez, K. A. Miller, T. Oki, Z. Sen, and I. A. Shiklomanov (2007), *Freshwater resources and their management. Climate Change 2007: Impacts, Adaptation and Vulnerability. Contribution of Working Group II to the Fourth Assessment Report of the Intergovernmental Panel on Climate Change*, edited by M. L. Parry, O. F. Canziani, J. P. Palutikof, P. J. van der Linden, and C. E. Hanson, Cambridge University Press, Cambridge, UK.
- Maupin, M. A., and N. L. Barber (2005), *Estimated Withdrawals from Principal Aquifers in the United States, 2000*, U.S. Geological Survey. [online] Available from: <http://pubs.usgs.gov/circ/2005/1279/pdf/circ1279.pdf> (Accessed 10 April 2010)
- Miller, N. L. (2003), *California Climate Change, Hydrologic Response, and Flood Forecasting*, International Expert Meeting on Urban Flood Management, Earth Sciences Division, Berkeley National Laboratory, World Trade Center Rotterdam, The Netherlands.
- Nightingale, H. (1975), Ground-Water Recharge Rates from Thermometry, *Ground Water*, 13(4), 340–345.
- NJDEP New Jersey Department of Environmental Protection (2004), *New Jersey Stormwater Best Management Practices Manual*, [online] Available from: http://www.njstormwater.org/bmp_manual2.htm (Accessed 19 April 2012)
- Roy-Poirier, A., P. Champagne, and Y. Filion (2010), Review of Bioretention System Research and Design: Past, Present, and Future, *Journal of Environmental Engineering*, 136(9), 878–889, doi:10.1061/(ASCE)EE.1943-7870.0000227.
- Schlea, D. A. (2011), Retention and management of stormwater runoff with rain gardens and rainwater harvesting systems, Ohio State University, Graduate Program in Food, Agricultural, and Biological Engineering.

SFPUC (2010), SFWATER.ORG : Low Impact Design, [online] Available from:
<http://sfwater.org/index.aspx?page=237> (Accessed 2 May 2011)

SFPUC and Wastewater Enterprise (2009), Low-Impact Design in San Francisco-LID Technical Workshop, [online] Available from:
<http://sfwater.org/index.aspx?page=314>

Stephens, D. B., M. Miller, S. J. Moore, T. Umstot, and D. J. Salvato (2012), Decentralized Groundwater Recharge Systems Using Roofwater and Stormwater Runoff1, *JAWRA Journal of the American Water Resources Association*, 48(1), 134–144, doi:10.1111/j.1752-1688.2011.00600.x.

Treidel, H., J. L. Martin-Bordes, and J. J. Gurdak (Eds.) (2012), *Climate change effects on groundwater resources: A global synthesis of findings and recommendations*, *International Association of Hydrogeologists (IAH) - International Contributions to Hydrogeology*, Taylor & Francis Publishing.

Tremblay, L., M. Larocque, F. Anctil, and C. Rivard (2011), Teleconnections and interannual variability in Canadian groundwater levels, *Journal of Hydrology*, 410(3-4), 178–188, doi:10.1016/j.jhydrol.2011.09.013.

2.0 Chapter 2—Recharge Beneath Low Impact Development

Understanding how low impact development (LID) site planning and integrated management practices (BMPs) affect recharge rates and volumes is important because of the increasing use of LID and BMP to reduce stormwater runoff and improve surface-water quality. Often considered a secondary management benefit, many BMPs may also enhance recharge to local aquifers; however these hypothesized benefits have not been thoroughly tested or quantified. In this study, I quantify stormwater capture and recharge enhancement beneath an BMP infiltration trench. Stormwater capture and retention was analyzed using the SCS TR-55 curve number method and in-situ infiltration rates to assess LID storage. Recharge was quantified using vadose zone monitoring equipment, a detailed water budget analysis, and a Hydrus-2D model. Additionally, the effects of historical and predicted future precipitation on recharge rates were examined using precipitation from the Geophysical Fluid Dynamic Laboratory (GFDL) A1F1 climate scenario. Predicted daily data was applied to a probability analysis examining the distribution of precipitation and runoff occurring during different precipitation scenarios including the interannual variability of the El Niño Southern Oscillation (ENSO). Results from this study indicate increased recharge under the GFDL A1F1 scenario compared with historical and GFDL modeled 20th century rates because of the higher frequency of large precipitation events that induce runoff into the infiltration trench.

Additionally, under a simulated A1F1 El Niño year, recharge would increase 6.9% compared with current El Niño recharge rates. In comparison, recharge was considerably lower beneath the grass lawn for historical and simulated precipitation years. This work highlights the strategic benefits of excess groundwater storage during ENSO years provided by LID sites while demonstrating the limitations of urban areas to handle excess water volumes introduced from climate variability.

3.0 Introduction

Surface and groundwater resources in many regions, especially urban, coastal environments are highly vulnerable to increasing human pressures, climate variability, and climate change [Green *et al.*, 2011; Treidel *et al.*, 2012]. Impervious surfaces such as buildings, roads, and parking lots prevent infiltration, increase contaminants in surface runoff that often overwhelm sewer systems, causing localized flooding, and combined stormwater-sewer flows that are often untreated, and reduce recharge to underlying aquifers. To address these problems, urban stormwater management practices are increasingly using low impact development (LID) site planning and integrated management practices (BMPs) to decrease the impacts on stormwater drainage systems, meet water-quality regulations that require new development maintain pre-development levels, and may eventually be used to help mitigate seawater intrusion [SFPUC and

Wastewater Enterprise, 2009]. Previous studies have reported a 40–90% peak runoff reduction using BMPs [Davis, 2008; Schlea, 2011]. LID and BMPs have the added benefit of constituent removal and attenuation, and can facilitate the use of polluted stormwater by incorporating the primary processes of passive volatilization, photodecomposition, adsorption, microbial biotransformation, and dilution, which require minimal energy and resources [Laws *et al.*, 2011]. BMPs are microscale and distributed management techniques that include the use of natural vegetated systems such as bioretention facilities, grassed/bioretention swales, and infiltration trenches to reduce, filter, and slow stormwater runoff, and are hypothesized to increase infiltration and recharge rates to aquifers [Nzewi *et al.*, 2010].

While the effectiveness of BMPs in reducing stormwater runoff has been documented [Dietz, 2005, 2007; Davis, 2008; Schlea, 2011], the effectiveness of BMPs in enhancing urban recharge is poorly understood, in part, because no field-based studies have directly measured recharge beneath an BMP [Davis *et al.*, 2009; Roy-Poirier *et al.*, 2010]. Understanding is further complicated in urban environments because recharge mechanisms, recharge enhancements compared to pre-development conditions, and the characteristics of subsurface flow processes are not well characterized [Lerner, 2002]. Sources of urban recharge include natural precipitation beneath permeable surfaces such as grass, irrigation on lawns and parks, leaking mains, sewers and septic systems, and water drainage systems

[Lerner, 1990; 2002]. To date, significant work has addressed the quality of water recharging BMPs [Dietz and Clausen, 2005, 2006, 2008]. However, the characteristics and quantities of subsurface flow beneath BMPs have been implemented with only hypothetical benefits, and these benefits have not been thoroughly field-tested for effectiveness in increasing recharge [Dietz, 2005; Dietz and Clausen, 2008; US EPA, 2000].

Previous studies have estimated recharge beneath BMPs as a percentage of precipitation. In the eastern United States, previous studies have estimated that between 50 and 98.8% of precipitation falling on the drainage area becomes recharge beneath BMPs [Dietz, 2005; Dietz and Clausen, 2006; Ermilio and Traver, 2006; Miller, 2006; Endreny and Collins, 2009; Stephens *et al.*, 2012]. Estimated recharge rates from a bio-retention study in semiarid New Mexico range from 0.076 to 1 m/year, which are orders of magnitude greater than natural recharge for that region [Stephens *et al.*, 2012]. The prior studies indicate that recharge beneath BMPs is likely a function of the runoff characteristics, precipitation intensity, and the storage capacity of the BMP facility and likely to have a dramatic effect on recharge [Shuster *et al.*, 2007]. Other studies have analyzed the effect of BMPs using groundwater models and have noted the large effect BMPs have on groundwater mounding, further documenting the large effect BMPs may have on recharge. However, no studies to-date have quantified in-situ

microscale LID recharge and how these features may impact recharge under climate variability [*Maimone et al.*, 2011; *Stephens et al.*, 2012].

Municipalities have implemented groundwater recharge studies for large scale managed aquifer sites and on an urban watershed scale, often using yearly water budgets and groundwater flow models to predict recharge [*Los Angeles and San Gabriel Rivers Watershed Council*, 2000; *City of Fresno*, 2012; *SFPUC*, 2012]. These studies do not address small scale or spatially distributed recharge beneath LID or the excess storage capacity provided by LID features during ENSO climate variability. An improved understanding of urban recharge, particularly beneath BMPs will guide adaptive management plans under growing populations and changing climate, particularly during intense precipitation events and climate variability.

It is well documented that interannual to multidecadal climate variability, such as the El Niño/Southern Oscillation (ENSO), substantially affects the magnitude and timing of precipitation, drought, runoff, and streamflow [*Cayan et al.*, 1992; *Dettinger and Cayan*, 1994; *Dettinger et al.*, 2001; *Enfield et al.*, 2001; *Labat*, 2008; *McCabe et al.*, 2004; *Vicente-Serrano et al.*, 2011]. ENSO is a coupled oceanic-atmospheric phenomenon that generally results in increased precipitation in some regions including California during the El Niño phase of the 2–6 year quasiperiodic cycle [*Wolter and Timlin*, 1993, 1998]. Furthermore, the effects of climate change on groundwater resources have been studied in recent

years [Earman and Dettinger, 2011; Green *et al.*, 2007, 2011; Treidel *et al.*, 2012; UNESCO, 2008]. Competing theories exist suggesting various feedback mechanisms in the Eastern Pacific may or may not reduce or enhance the sea-surface temperature gradient [Wang *et al.*, 2012]. There is great uncertainty in the response of the Eastern Pacific to climate change and there is a lack of robust evidence to suggest a stronger or weaker ENSO in the next century [Wang *et al.*, 2012]. Recharge rates and mechanisms and corresponding groundwater levels beneath natural and agricultural lands, however, do respond to interannual to multidecadal climate variability from ENSO and other oceanic-atmospheric phenomenon [Gurdak *et al.*, 2007, 2009; Holman *et al.*, 2009, 2011; Tremblay *et al.*, 2011]. Estimating the capacity for managed recharge of excess surface water from climate variations is an important step for the conjunctive and sustainable use of surface and groundwater resources.

The purpose of this chapter is twofold. First, I quantify and compare recharge rates and volumes beneath a recently installed (2009-2010) BMP infiltration trench compared with an irrigated grass lawn that represents a typical urban location of recharge, and I evaluate the controlling factors on recharge beneath the two sites. Secondly, I simulate historical and future ENSO precipitation scenarios to evaluate the effectiveness of the BMP infiltration trench in capturing runoff and enhancing recharge. This study provides the first field- and model-based estimates of recharge rates and volumes beneath BMPs under

climate variability, and offers useful information regarding enhanced stormwater capture and recharge for improved water-resource management in urban environments.

4.0 Study Area Description

The study area includes a recently (2011) instrumented BMP infiltration trench and irrigated lawn located within the city of San Francisco, California, USA and above the Westside Basin aquifer (104 km²), which is part of the regionally important California Coastal aquifer system (Figure 1). The Westside Basin aquifer system has a shallow (< 30 m below sea level), unconfined aquifer and two deeper confined aquifers, and is bounded in the north and south by Franciscan Complex bedrock [*Clifton et al.*, 1988; *Nzewi et al.*, 2010]. The aquifer sediments include coastal deposits of sand, silt, mud, gravel, and peat from the Merced and Colma Formations. Based on a county-wide groundwater flow model, *Phillips et al.* [1993] reported 200 mm/year as a spatially averaged estimate of natural and urban induced recharge to the Westside Basin aquifer. While the Westside Basin aquifer is not the primary source of drinking water for San Francisco, groundwater from the aquifer is used by a number of neighboring communities and seawater intrusion has been a localized problem in the southeastern part of the aquifer [*Nzewi et al.*, 2010]. Additionally, the San Francisco Public Utilities Commission (SFPUC) has proposed constructing up to

six new public and emergency supply wells in the Westside Basin aquifer that could supply approximately 4 million gallons of water per day to supplement the primary surface-water supply [Nzewi *et al.*, 2010].

The effects of ENSO on spatiotemporal patterns of precipitation and runoff in California are well documented [Dettinger *et al.*, 2001]. In a study of daily maximum precipitation rates for California, Shang *et al.* (2011) found that large precipitation events (defined in the study as 50-year return interval of approximately 150 mm) were strongly correlated with ENSO variability. The frequency of central pacific and eastern pacific ENSO events have increased in recent decades and may be attributed to natural variability [Yeh *et al.*, 2011]. Additionally, daily precipitation maximums have increased by 6.5% per decade for urban areas in California [Mishra and Lettenmaier, 2011]. The natural variability of ENSO and the projected increases in precipitation maximums have important implications for recharge to aquifers, especially those in California. As the probability distribution of precipitation changes and possibly includes more intense events, LID and BMPs may play a critical role in capturing the runoff and promoting recharge that would otherwise be lost to the stormwater system.

Global circulation models (GCMs) can also provide information about California's future precipitation patterns. GCMs typically predict future temperature, precipitation, and wind speed. In California, GCMs have predicted precipitation increases however there is still much debate regarding ENSO

forecasted changes [Miller, 2003; IPCC, 2007; Pierce et al., 2012]. In an increased precipitation scenario for a region such as California, higher rates of rainfall over a shorter period of time may not necessarily translate into more recharge. Under such conditions, the aquifer might not be able to capture the excess water for storage because the maximum infiltration capacity has been reached and recharge is limited when much of the precipitation remains as surface runoff [UNESCO, 2008].

5.0 Methods

5.1 Vadose Zone Data Collection

San Francisco State University, located in the lower southwest of San Francisco, is the home of many new LID features including an LID infiltration trench. The area of the trench is approximately 10.8 m² (12 m x 0.9 m) located in the center of a vegetated depression that funnels runoff from an impervious bike path and surrounding roof tops with a maximum drainage area of 1,400 m² (Figure 1). Four distinct lithologic units were visually identified at the infiltration trench (Figure 2), and six sediment cores were characterized by a sediment textural analysis for %sand-%silt-%clay-%gravel [Alpha Analytical Labs, 2012]. At the downstream end of the infiltration trench is an overflow drain with a 3-cm

diameter weephole that discharges water when the trench reaches the maximum storage capacity of approximately 2.0 m^3 .

The irrigated grass-lawn site was defined as a 4.0 m^2 circle surrounding the vadose-zone monitoring equipment. This site is located approximately 500 m away from the LID infiltration trench and was chosen to represent background recharge conditions for a typical urban setting. At the grass-lawn site, two distinct visual lithologic units were identified (Figure 2), and five sediment cores were characterized for the sediment textural analysis. The grass lawn site is not conducive to surface runoff from surrounding vegetated areas because of the slope at the site

Each site was instrumented with five Decagon 5TM soil moisture sensors, five Decagon MPS-1 matric potential sensors, and one Decagon G2/G3 drain gauge (Figure 2) [Decagon Devices, 2012]. The Decagon G3 drain gauge located at the infiltration trench collects water volumes that must be pumped out at daily intervals with a hand-pump. The Decagon G2 at the irrigated lawn site has an automated data logger that measures a water volume every five minutes using a tipping bucket method. Each water volume is converted to a water flux by the sensor in dimensions of L T^{-1} . Additionally one Decagon ECRN-100 rain gauge, one Solinst Inc. barometer, and three piezometers with Solinst Inc. pressure transducers were installed at the infiltration trench site [Solinst Inc., 2011]. The piezometers were installed at three locations within the infiltration trench at the

base of the gravel layer. Each piezometer was constructed of pvc pipe with a slotted screen and extended to 25 cm above the gravel layer. A monitoring well with a short screen (< 2 m) was installed near the perched water table (2.13 m bls) at the infiltration trench to record fluctuations in deep water levels. The Decagon sensors began collecting data on June 19, 2011, and the pressure transducers began collecting data on January 4, 2012.

I calculated bulk density following the methods of *McMahon et al.* [2003], and further defined the soil parameters by constructing water retention curves. A water retention curve relates the water content, matric potential, and hydraulic conductivity of the soil type. I first built each water retention curves in RETC, a program used to analyze the hydraulic conductivity and soil water retention functions of unsaturated soils using soil texture data [*van Genuchten et al.*, 1991]. I then corrected the water content and hydraulic conductivity curves for the gravel content using the procedure outlined by *Bouwer and Rice* (1984).

5.2 Climate Variability

5.2.1 *Historical Precipitation*

Historical daily precipitation data from the San Francisco, Mission Dolores station (1914-2012) were evaluated to assess statistical differences between El Niño and La Niña winter precipitation and to analyze the potential recharge differences between the BMP and the irrigated lawn site [*NOAA NCDC*,

2011; *WRCC*, 2012]. Hourly precipitation data are only available from 1948-present. All precipitation datasets were aggregated to hourly, daily, and monthly intervals and statistical differences between historical El Niño and La Niña precipitation were analyzed at all three time intervals using a Kruskal-Wallis test [*Helsel and Hirsch*, 2002; *Crawley*, 2007]. ENSO years and the intensity recorded on the Multivariate ENSO Index (MEI) were obtained from NOAA [*NOAA ESRL*, 2012; *NOAA*, 2012]. Precipitation datasets were separated into four categories: 1) 2011-2012; 2) Average historical; 3) Historical El Niño, and 4) Historical La Niña. Probability distributions for each category were then evaluated (discussed below). Monthly total precipitation for the study site including ENSO years is shown in Figure 3.

5.2.2 *Future Precipitation Scenarios*

Simulated future precipitation was obtained from the Geophysical Fluid Dynamics Laboratory (GFDL) A1F1 climate model run to analyze changes in future precipitation intensity and duration [*NOAA GFDL*, 2012]. The A1F1 scenario represents a world that remains reliant on fossil fuels leading to a best estimate temperature rise of 4.0°C from 1990 levels by 2100 [*IPCC*, 2007]. Future precipitation changes from 2000 to 2100 were assessed using a linear mixed-effects model (LME) to statistically determine the magnitude of precipitation changes in the future compared with GFDL modeled results from the

20th century (1861-2000) [Crawley, 2007]. A delta-factor method downscaling approach was used in this study to statistically transform the large spatial scale (1° latitude-1° longitude) data to represent a localized predicted dataset for San Francisco. Precipitation data from the GFDL 20th century and the 21st century A1F1 models is shown in Figure 4.

To analyze the percent change in future precipitation, the percent change in daily precipitation was calculated two ways: by month and by intensity between the GFDL 21st A1F1 and GFDL 20th century model using the delta-factor method [Taylor and Tindimugaya, 2012]. In previous studies, daily precipitation changes are usually reported as one percentage change for the future and that value is typically applied to all precipitation throughout the year (e.g. precipitation will increase by 20% in the future) [Barbu *et al.*, 2008; Pyke *et al.*, 2011]. By evaluating how daily precipitation is changing in the future by month or by the intensity group, I can better estimate how forecasted precipitation will change for typically strong ENSO months (December-March). Summary statistics were run on both groups of data, then analyzed by month using a Kruskal-Wallis Test [Helsel and Hirsch, 2002; Crawley, 2007].

To create a forecasted precipitation dataset at the local level for San Francisco, I applied the monthly % changes predicted by the GFDL model to the historical SF Mission Dolores datasets using the delta-factor method [Taylor and Tindimugaya, 2012]. This provided linearly scaled precipitation that increased or

decreased for each month as predicted by the GFDL. This method assumes a similar frequency and timing of events and only simulates future intensity changes. Once I had the forecasted precipitation dataset, I separated the data into three categories: 1) Simulated GFDL A1F1; 2) Simulated El Niño; and 3) Simulated La Niña. Exponential probability distributions were created for all three previously mentioned climate categories.

Differences in precipitation intensity between the GFDL 20th century and GFDL A1F1 21st century were also analyzed for statistical differences between low and high intensity groups. Data were separated into two categories: low (daily precipitation < 8 mm) and high (daily precipitation > 8 mm). This distinction between low and high precipitation was obtained from the probability density curves which show a distinct axis of shift around 8 mm of daily precipitation. Once values were separated into their two groups, statistical differences were analyzed with a Kruskal-Wallis test.

An LME model was used to test for significant differences in the precipitation values between the GFDL modeled 20th century historical dataset and the GFDL 21st century future precipitation datasets [Crawley, 2007]. An LME model takes into account temporal pseudo-replication which is a feature of seasonal data such as precipitation. In this case, a linear regression model would wrongly suggest an increasing trend in precipitation. The LME model takes into account fixed and random effects; in this case time represents the explanatory

variable and the data is analyzed with and without this variable as a fixed and random effect. The model is run with and without time as a fixed (α) and random effect (ε) to determine if the change in precipitation actually occurs with time or if a similar distribution of precipitation would occur if time was placed in a random order (Equation 1).

$$y = \alpha + \beta\sin(2\pi t) + \gamma\cos(2\pi t) + \varepsilon \quad [1]$$

This model was run three times to evaluate the difference that the explanatory variable (time) contributes to the overall precipitation trend: 1) time as a fixed effect; 2) time as a fixed effect and random effect; 3) no fixed effect and time only as a random effect. An ANOVA analysis was subsequently run between the three LME models to determine the statistical significance of time as a predictor of precipitation change [*Helsel and Hirsch*, 2002; *Crawley*, 2007]. The LME model tests for a long-term precipitation trend and does not provide evidence for inter-annual changes between months.

5.3 Stormwater Capture Capacity

I evaluated the capacity of the BMP infiltration trench to capture and store runoff under 2-, 5-, 10-, 25-, and 50-year precipitation return intervals to determine the threshold of overflow from the trench under specified rain events. Precipitation return intervals were determined from standard exceedence probabilities and depth-duration-frequency curves. Precipitation return intervals

for the study site from the entire time period (1914-2012) are shown in Table 1. Stormwater capture capacity (SCC) is here defined as the ratio of stormwater capture and retention (volume captured L^3) to total stormwater inflow (volume inflow L^3). Once the maximum capacity of the trench has been reached, water begins to flow out of the infiltration trench into the overflow drain via a weephole. All remaining water in storage eventually infiltrates and may become recharge if not lost to evaporation. To calculate the volume of stormwater in the gravel trench during each hour of a storm, I used an hourly water budget that accounts for incoming precipitation, runoff, and outgoing overflow. The instantaneous storage gained during each hour is shown by equation [2]:

$$S = P + R_{off} - O_f \quad [2]$$

where S is the volumetric storage gained in the gravel after overflow [$L^3 T^{-1}$] during each hourly time interval, P is precipitation [$L^3 T^{-1}$] from the Mission Dolores station falling directly on the gravel trench, R_{off} is runoff [$L^3 T^{-1}$], O_f is overflow out of the trench which occurs when water levels are greater than the maximum storage capacity of approximately $2.0 m^3$ [$L^3 T^{-1}$]. The total change in storage for the storm is calculated by taking the sum of the gain in storage for the gravel trench during each time interval. The SCC is then calculated by taking the ratio of the total gain in storage in the gravel (stormwater retention) to the total water inflow ($P + R_{off}$) shown by equation [3].

$$SCE = \frac{S}{P+R_{off}} * 100 \quad [3]$$

Runoff (R_{off}) was used in four sections of this analysis: 1) stormwater capture capacity (equations 2 and 3); 2) water-budget recharge method; 3) modified water-budge method using precipitation probability; and 4) Hydrus-2d recharge method. Daily and hourly runoff to the infiltration trench was calculated for the period 2009 to 2012 using the TR-55 SCS curve number method [*Natural Resources Conservation Service, 1986*]. A curve number of 98, representing impermeable surfaces such as roofs and pavement was applied to the impermeable surfaces draining to the trench. The runoff (R_{off}) used in equation 2 and 3 is calculated using equation [4] as shown below.

$$R_{off} = \frac{\left[P - 0.2 \left(\frac{100}{CN} - 10 \right) \right]^2}{\left[P + 0.8 \left(\frac{100}{CN} - 10 \right) \right]} \quad [4]$$

Where R_{off} is the runoff [$L T^{-1}$], P is the precipitation [$L T^{-1}$], and CN is the composite curve number (unitless). I estimated an effective drainage area of 430 m^2 based on the runoff values and calibrated to observed water levels during a large precipitation event. It should be noted that large discrepancies can occur when using the runoff curve number method for hourly precipitation values $< 1 \text{ mm}$ [*Natural Resources Conservation Service, 1986; Pitt, 1999*].

Overflow (O_f) was calculated in two-steps. First, the maximum overflow from the 3-cm diameter weephole was calculated at $7.58 \text{ m}^3/\text{hour}$ using Toricelli's

Law and Bernoulli's Equation, which are standard physics equations for modeling flow from a point source and assume pressure head does not have an effect on the drainage rate because of the presence of gravel [Dingman, 2002]. Second, hourly outflow from the weephole was assumed to equal hourly water inflow (R_{off} and P) provided the water in the trench had exceeded the maximum storage capacity of approximately 2.0 m^3 and the water inflow was less than the maximum outflow.

The total water storage gained in the gravel trench is assumed to eventually become infiltration. The infiltration rate beneath the trench is a function of the saturated hydraulic conductivity value for the soil beneath the gravel. This rate was calculated using in-situ water level data in the gravel trench during ponded conditions after a rain event and after runoff ended. The saturated hydraulic conductivity was found to be less in-situ than that derived by the water retention curves and the in-situ value was therefore used as the infiltration value for the ponded conditions. At the grass lawn site, the sources for infiltration are precipitation [L/T] and in-situ irrigation [L/T]. In-situ irrigation rates were measured using a specialized irrigation audit and is less than the saturated hydraulic conductivity [The Irrigation Association, 2010]. Irrigation rates were then used as the maximum infiltration rate. Once ponding was initiated, the saturated hydraulic conductivity value was applied. Precipitation and irrigation contribute to infiltration at the irrigated lawn site until ponding occurs and excess water becomes runoff. There is no surface runoff to the lawn site.

5.4 Recharge

Recharge is the vertical and volumetric flux of water across the water table and expressed as volume per time (cubic millimeters per year) or more commonly as length per time (such as millimeters per year). Recharge is one of the most difficult water-budget components to quantify because of its spatial and temporal variability [McMahon *et al.*, 2011]. Using a wide variety of approaches to estimate recharge has been shown to reduce uncertainties and increase confidence in recharge estimates [Scanlon *et al.*, 2002a]. Therefore, I estimate recharge using the following five methods: 1) Darcy method; 2) In-situ drainage; 3) Hydrus-2D; 4) Water budget; 5) Water budget from future precipitation and runoff probability.

5.4.1 Darcy Method

Recharge rates were estimated using the 1-dimensional Darcy method [Healy, 2010] and equation [5]:

$$R = K_s * K_r(h) * \frac{\partial H}{\partial z} \quad [5]$$

where R is recharge [L T⁻¹], K_s is the vertical saturated hydraulic conductivity [L T⁻¹], K_r(h) is the unsaturated hydraulic conductivity coefficient at the ambient pressure head, h; H is total head [L]; and z is depth below land surface [L]. All input values were derived from the previously described field instrumentation and

from water retention curves built from a sediment textural analysis of the sediment cores.

5.4.2 *In-situ Drainage*

I collected the drainage volume [L^3] from the drain gauge beneath the infiltration trench on an approximate daily schedule. The drainage volume was converted to a flux by dividing by the area of the drain gauge (25.4 cm^2). At the irrigated grass lawn site, the drain gauge records a water drainage flux every five minutes [$L \text{ T}^{-1}$] with a data logger. I assume that water collected in the drainage gauge beneath the infiltration trench and lawn site are representative of recharge values.

5.4.3 *Hydrus-2D*

I estimated recharge rates using a Hydrus-2D model [Simunek *et al.*, 2008; PC-Progress, 2011] that I calibrated based on observed total potential and water content field data. Hydrus-2D is a computer program that numerically solves the Richards equation [Richards, 1931] for saturated and unsaturated water flow and Fickian-based advection-dispersion equations for heat and solute transport [Dingman, 2002; Simunek *et al.*, 2008].

The infiltration trench model domain was constructed using a 2.4 m x 3.0 m cross section of the infiltration trench with 63,000 2D-finite elements and a mesh size of 0.03 m (Figure 5). The Hydrus-2D mesh was designed to capture the intrinsic changes that occur at soil boundaries by reducing the mesh size to 0.01m at soil boundaries—especially important at the gravel-sand boundary. A 2.0 m x 2.0 m model domain was constructed for the irrigated grass lawn. The cross section contained 45,000 2D-finite elements and the same mesh size as the infiltration trench (Figure 5). Five soil layers were included in both the infiltration trench model and irrigated lawn model. Associated van Genuchten parameters for each soil type are shown in Table 2 and Table 3 respectively.

Both models were initialized to steady state using constant head boundary conditions for 50 days. The infiltration trench was initialized with a constant upper-head boundary of -0.94 m and a constant bottom-head boundary of -0.2 m with pressure head increasing linearly with depth representing values obtained from the field matric potential sensors. The irrigated grass lawn was initially modeled using a constant upper-head boundary of -0.90 m and a constant bottom-head boundary of -0.50 m. Steady-state runs were initialized for both models at a minimum time step of 1 second. The output pressure head field was then used as initial conditions for the transient simulations.

Recharge was then estimated by running transient precipitation scenarios and averaging the volumetric flux at the bottom of the model domain for each

year. A 1-year transient simulation with an hourly time-discretization was run for the irrigation trench using precipitation, runoff, evaporation, and irrigation as time-variable parameters for the year 2011-2012. A 12-year transient simulation (2000-2012) was run for the grass lawn at a daily time-discretization with precipitation, irrigation, soil evaporation, and evapotranspiration used as time-variable conditions. After the transient simulations produced recharge values within reasonable tolerances to the other four methods, transient simulations with future predicted precipitation, based on the linearly transformed Mission Dolores dataset and runoff values for the year 2100 were input into both models.

5.4.4 *Water-Budget Method*

The water-budget method [Healy, 2010] was used to estimate recharge beneath the infiltration trench and the lawn sites, and incorporates precipitation, irrigation, evaporation, transpiration, runoff from impermeable surfaces, and changes in storage. In simplified form, recharge from a water budget is estimated using equation [6]:

$$R = P + R_{off} + I - ET - O_f - \Delta S \quad [6]$$

where R is recharge [$L T^{-1}$], P is precipitation [$L T^{-1}$], R_{off} is runoff from the paved surfaces [$L T^{-1}$], I is irrigation [$L T^{-1}$], ET is evapotranspiration [$L T^{-1}$], O_f is overflow out of the trench, which occurs when water levels are above capacity

[L T⁻¹], and ΔS is change in storage in the soil [L T⁻¹]. P, R_{off}, and I are inputs to the system and ET and O_f are outputs. In this study, the change in storage of the system (ΔS) was negligible because water contents remain relatively stable and lacks a zero-flux plane as is typical of semi/arid-environments [Healy, 2010]. Hourly intervals were used for the infiltration trench and daily intervals were used for the grass lawn.

Runoff flowing into the infiltration trench was evaluated using the curve number and runoff methods as described previously. Irrigation for the grass lawn was calculated as 3.1 cm/hour (or approximately 2.79 cm/week at 54 minutes of irrigation total per week) using the methods outlined in a specialized irrigation auditor manual [*The Irrigation Association*, 2010]. Irrigation rates for the infiltration trench were provided by SFSU Facilities personnel and estimated as approximately 2.4 cm/week.

Evapotranspiration was separated into two variables: soil evaporation and plant evapotranspiration. Soil evaporation was calculated using the method outlined by *Kay and Davies* (2008). Many equations have been developed to estimate evaporation using simple meteorological variables. The most simple of these is a modified version of the Penman-Monteith equation shown by equation [7] [*Kay and Davies*, 2008]:

$$PE = \frac{R_e*(T+5)}{\lambda*\rho_w*100} \text{ for } T > -5 \quad [7]$$

where PE is the potential evaporation [m/day], R_e is the extraterrestrial radiation [J/m²/s], T is the mean daily air temperature [°C], λ is the latent heat of vaporization [2.45E6 J/kg], and ρ_w is the density of water [kg/m³].

Evapotranspiration is a separate variable from soil evaporation and was calculated for the irrigated grass lawn using a simple empirical coefficient approach shown in equation [8] [*California Department of Water Resources, 2000; Romero and Dukes, 2009*]:

$$ET = K_L * ET_0 \quad [8]$$

where ET is the evapotranspiration [m/day], K_L is the landscape coefficient (unitless), and ET_0 is the reference evapotranspiration for San Francisco (m/day). Reference values of K_L range between 0.5-0.8. Reference values for San Francisco ET range from 1.27-3.56 cm/month in July and are estimated to decrease in a Gaussian distribution for the six months prior to and after July to values of approximately 1-2 cm/month in December and January.

From the water budget analysis (equation 6), the percent of total water inputs to the LID that becomes recharge can be calculated using equation [9]:

$$\% \text{ recharge} = \frac{\text{Inputs} - \text{Outputs}}{\text{Inputs}} * 100 \quad [9]$$

where the inputs [L T⁻¹] and outputs [L T⁻¹] were previously defined in equation 5. The % recharge is used to evaluate recharge rates under future precipitation and runoff-probability scenarios.

5.4.5 *Water budget from future precipitation and runoff probability*

Historical runoff and recharge probabilities for the BMP were assessed using historical precipitation values applied to a cumulative probability method [Department of Environmental Resources, 1999, 2007]. Probability and cumulative probability methods are standard statistical procedures [Helsel and Hirsch, 2002; Crawley, 2007] and were previously demonstrated in a runoff analysis applied to a BMP in Maryland [Department of Environmental Resources, 1999, 2007]. The cumulative precipitation probability function is shown by equation [10] [Helsel and Hirsch, 2002; Crawley, 2007]:

$$F(p) = \int_0^{P^{max}} \lambda e^{-\lambda p} dp, p \geq 0 \quad [10]$$

where $\lambda=1/\mu$ is an exponential coefficient, μ is the mean of the exponential precipitation dataset, p is the daily precipitation [L/T]. Cumulative yearly precipitation and runoff are used as input values to a modified water budget to predict a yearly recharge value. The modified water budget is shown in equation [11]:

$$R = (P + R_{off} + I) * (\% \text{ recharge}) \quad [11]$$

where R , P , R_{off} , I , and $\%$ recharge were previously defined in equations 6 and 9. Forecasted precipitation and runoff associated with yearly rain events from simulated GFDL A1F1 21st century, simulated A1F1 El Niño, and simulated

A1F1 La Niña type rain events were calculated using the probability function. Cumulative values were then input into equation [11] to calculate a predicted recharge rate. Historical and forecasted probable recharge values were then compared to analyze the forecasted change in recharge relative to both precipitation distributions.

The probability method provides the total yearly cumulative probable volume of water that drains into the system given the distribution of precipitation for each precipitation category. This method also provides a way for analyzing the change in recharge rates relative to the precipitation distributions.

6.0 Results and Discussion

Results presented in this section transition from analysis of the field data and the stormwater capture capacity of the system to the final recharge results as calculated by all five methods. The initial results provided in the field data analysis and the stormwater capture capacity sections provide a context to the recharge rates presented in the final section.

6.1 Time series of water content and matric potential

Daily total potential and water content for the infiltration trench are shown in Figure 6 and 7. The observed total potential profiles approach unit gradient ($dH/dz = -1$) beneath the infiltration trench (-1.01 m/m) and the grass lawn (-1.02

m/m) and indicate a constant downward flux of water driven by gravity beneath each site [Healy, 2010]. When total potential profiles are shown over time (Figure 8), total potentials do not demonstrate a sharp and uniform wetting front during precipitation events. A data-sensor malfunction is seen in the uppermost sensor and the sensors directly below (0.41 m and 0.61 m below the gravel) show no appreciable fluctuations with wetting events. The fluctuations in total potential at the bottom sensor 1.23 m below the gravel show appreciable fluctuations and this is a function of the perched water table that is approximately 1.47 m below the base of the gravel layer. Irrigation at the site provides a daily source of water to the infiltration trench keeping the matric potential values low (saturated) and obscuring large changes due to precipitation.

Water contents for the infiltration trench are shown in Figure 7. Shifts can be seen approximately daily from the sensors 0.03 m and 0.41 m below the gravel base and this is due to irrigation surrounding the infiltration trench. Large changes in water contents are observed approximately twice per month. This is most likely due to large volumes of water that have entered the trench during precipitation events and have remained in storage in the gravel layer as well as from large irrigation values that occur uphill from the trench and cause ponding in surrounding areas.

6.2 Historical Precipitation

Maximum daily and hourly event-based precipitation statistics (mm/hour and mm/day) are shown in Table 4. The hourly mean average precipitation was 1.35 mm/hour, however the maximum value ever recorded at this station was 44.7 mm/hour which occurred on January 23, 1963. Daily mean precipitation was 10.9 mm/day with a maximum value of 140.7 mm/day occurring on the same day as the maximum hourly occurrence. Both datasets are strongly skewed about the mean with skewness values of 4.36 and 2.69 for the hourly and daily data respectively. Difference in daily precipitation between El Niño and La Niña was analyzed using the non-parametric Kruskal-Wallis test for significant differences between populations. Results of the Kruskal-Wallis test (chi-squared = 4.28, df = 1, $p = 0.038$) indicate a statistically significant difference in daily precipitation between the El Niño and La Niña years.

6.3 Future Precipitation Scenarios

The LME model applied to the GFDL dataset predicts a net precipitation decrease of -0.14 mm in daily precipitation from 1861 to 2100. The ANOVA analysis between the three LME models (with and without fixed and random effects) indicates that the decrease of -0.14 mm per day is not statistically significant at the $p = 0.05$ level ($t = -0.366$, $p = 0.715$). When accounting for time as a random and fixed effect, there is no apparent statistical evidence to support

an increasing or decreasing trend in total daily precipitation over the 21st century with the A1F1 scenario.

While the long-term trend predicted by the linear-mixed effects model does not predict significant net daily precipitation changes for the 21st century, the percent change in daily precipitation when separated by month was found to be statistically significant for more than 10 months throughout the year as shown by the Kruskal-Wallis test in Table 5. Only February and March are forecasted to have no statistically significant change in daily precipitation over the 21st century as predicted by the GFDL A1F1 model. All other months show statistically significant changes at the $p = 0.05$ level (Table 5). Forecasted precipitation aggregated by season indicate a change of +8%, -8%, -19%, and -6% for DJF, MAM, JJA, SON respectively in daily precipitation. *Pierce et al.* [2012] indicate similar changes of +2%, -18%, -15%, and -5% for DJF, MAM, JJA, SON respectively. Changes between low daily precipitation intensity (< 8 mm) and high daily precipitation intensity (> 8 mm) were also analyzed between the GFDL 20th century dataset and the GFDL A1F1 21st century dataset and are shown in Table 6. Low intensity events are predicted to decrease by -3.2 % ($\chi^2 = 3.87$, $p = 0.04$) while high intensity events are predicted to increase by +11.2% ($\chi^2 = 30.92$, $p < 0.01$).

6.4 Stormwater Capture Efficiency

To better understand the limiting threshold of the infiltration trench to capture and retain runoff under maximum storm scenarios, I conducted a stormwater capture efficiency analysis for over 100 different storms of varying magnitudes. A maximum example was simulated for the largest recorded daily precipitation event (50-year return interval of 140.7 mm) occurring on November 5-6, 1994, which was a moderately strong El Niño year (+1.3) [NOAA ESRL, 2012]. The input, output, and storage volumes during the November 5-6, 1994 storm are shown in Figure 9.

The November 5-6, 1994 event generated a maximum hourly precipitation of 18.2 mm/hour, 170.1 mm of total precipitation, and 36.89 m³ in runoff to the infiltration trench. The infiltration trench would have filled to capacity after 16 hours of moderately continuous precipitation (<5 mm/hour) shown in Figure 9 around 4 PM. The trench continued to overflow and infiltrate water during 11 hours of moderately high precipitation (>7 mm). The infiltration trench had a stormwater capture efficiency of only 11.9% (4.4 m³) of the stormwater runoff (shown by the area between the curves which is the shaded region in Figure 9) and discharged the remaining 32.5 m³ as overflow into the stormwater system. In the 1994-1995 water year, there was 864 mm of total annual precipitation and 53.6% (50.3 m³) of stormwater capture efficiency in the infiltration trench for the entire year. In contrast, relatively low-intensity precipitation events result in a comparatively higher percentage of stormwater capture, but lower overall volume

as compared to higher-intensity events. For example, a 2-5 year storm in March, 2012 with 56 mm of total precipitation of over 1 day, the trench captured 61.5 % (3.4 m^3) of the total runoff. During the period of field observations (2011 to 2012), all of the daily precipitation events were at or below the 2-5 year design storm values ($< 45 \text{ mm/day}$), resulting in 374.8 mm of total annual precipitation and 79.2% (20.8 m^3) of annual stormwater capture. Although the percentage of stormwater capture in the infiltration trench is inversely related to the storm intensity, the total volume of stormwater capture, and thus water available for infiltration and recharge beneath the trench, directly increases as storm intensity increases (Figure 10).

6.5 Runoff

The probable runoff volume associated with the daily precipitation probability for the GFDL A1F1 20th century and 21st century scenarios are shown in Figure 11. The GFDL A1F1 model predicts differences in precipitation intensity, shifting the precipitation probability to include a higher probability of larger intensity events as compared to the 20th century GFDL predictions. The probable runoff volume is the volume of runoff associated with each precipitation value and scaled by the precipitation probability. This shift in the probability of the daily rain events translates into a large difference in the runoff probability distribution (a shift of approximately +16.6% in peak probable volumetric runoff).

A higher probability of larger magnitude events will translate into larger runoff values. Low intensity events (<1 mm/hour) do not produce runoff yet historically constitute 25% of the total rainfall events that occur each year. Low intensity events (<1 mm/hour) which previously did not initially contribute to runoff may decrease in frequency over the 21st century and shift to higher intensity events and subsequently contribute to more runoff in the future.

6.6 Recharge

Table 7 shows recharge rates calculated by the five recharge methods, and provides one predicted value of future recharge as modeled by Hydrus-2D. Historical recharge rates are an order of magnitude greater beneath the infiltration trench (1,623 to 5,111 mm/year) as compared to rates beneath the grass lawn site (130 to 511 mm/year) (Table 7). For the infiltration trench, the water budget using the rainfall-runoff probability curves predicts much higher recharge rates than the other methods for 2011-2012. This result could be influenced by larger predicted runoff volumes than are actually found at the site which is a function of the effective area of runoff. For one year, a recharge rate of 200 mm/year [*Phillips et al.*, 1993], under a naturally vegetated site of 430 m² would produce approximately 86 m³ of recharge volume. When comparing this to the derived volumes beneath the BMP, yearly volumes do not compare with pre-development recharge values.

Recharge rates estimated from the 1-D Darcy method (2,344 and 551 mm/year) are generally greater than the in-situ drainage rates (1,623 and 130 mm/year), respectively beneath the infiltration trench and grass lawn (Table 7). The difference in estimated recharge rates between the two methods is caused by the increase in bulk density and corresponding decrease in porosity upon repacking the native sediment in the in-situ drainage gage during installation. Recharge predicted by Hydrus-2D for 2011-2012 are 2,582 and 409 mm/year for the infiltration trench and grass lawn respectively. The cumulative flux (representing the yearly recharge value) at the bottom free drainage boundary of the infiltration trench and grass lawn within Hydrus-2D is shown in Figure 12. Results from the water budget method are shown in Figure 13. Recharge is significantly greater beneath the infiltration trench because of the greater quantity of water entering the infiltration trench system from runoff. The greatest source of water for the grass lawn is from irrigation, however much of that is eventually lost to ET. From the 2011-2012 water budgets, the percent recharge is 63% and 10.5% of the total water inputs to the infiltration trench and the grass lawn, respectively. The percentage of recharge beneath the infiltration trench varies from 30% to 80% depending on the intensity of storms and the year in which it occurs.

Recharge predictions calculated from the modified water budget using the probability analysis for all eight precipitation scenarios are shown in Table 8 and Table 9 for the infiltration trench and the grass lawn, respectively. Historical

recharge probabilities for an average year from 1914-2012 for San Francisco were found to be 5,260 mm/year beneath the irrigation trench and 170 mm/year beneath the lawn site. When comparing historical values to the simulated GFDL A1F1 locally-modified dataset for the infiltration trench, recharge rates would increase approximately 100 mm/year. This recharge increase would occur because of the increase in lower probability, large intensity precipitation events. Low intensity precipitation events do not induce runoff and the shift in the probability curve from low-intensity to high-intensity events indicates runoff would be the dominant driver of recharge in this system. Recharge is not predicted to increase for the grass lawn.

When comparing historical and future predicted ENSO events, the probability analysis indicates that future El Niños are likely to increase recharge beneath the infiltration trench by 1.35% (from 6,620 to 6,710 mm/year, Tables 8 and 9). Recharge rates are also predicted to increase for future La Niña by 1.5% from 4,530 to 4,600 mm/year (Tables 8 and 9). Recharge rates are not predicted to increase for the grass lawn because these systems are not gaining enhanced water inputs from surface water runoff. The simulated increase in recharge rates is due to the shift in the distribution of precipitation intensity from low intensity to a greater frequency of higher intensity events. The timing of storms with respect to other storms in any given year also influences recharge rates beneath the BMP.

Understanding how the timing of future storms and ENSO variability may change will further improve recharge calculations for this site.

7.0 Conclusions

Using a variety of methods, recharge was quantified and compared between a BMP infiltration trench and an urban, irrigated grass lawn. Recharge was found to be greater beneath the infiltration trench, and on average the trench recharges approximately 33% of all water input to the trench system (precipitation, irrigation, and runoff). In contrast, recharge beneath the grass lawn was approximately 10% of water input (precipitation and irrigation only). Predicted daily precipitation values show statistically significant differences from modeled historical precipitation to modeled A1F1 predicted precipitation when analyzed by month. Based on the anticipated daily precipitation changes, average probability distributions of precipitation from historical and predicted ENSO years were analyzed, and runoff probability distributions were calculated and used for assessing predicted changes in recharge. Historical and predicted El Niño years demonstrate higher recharge rates compared with historical average years or La Niña years. Simulated precipitation probability for both El Niño and La Niña shows greater predicted recharge under both scenarios at the LID infiltration trench site. Noticeable differences in recharge are not predicted for the grass lawn site because there is no runoff entering the site. Based on the storage capacity, the

infiltration trench has a stormwater capture efficiency of between 40-100% for storms at or below the 5-year return period which is larger than the range 50- 80% previously reported.

As population continues to rise in the future, adaptation approaches such as LID will become vital as water resource management tools, particularly for urban, coastal aquifers that are susceptible to sea-water intrusion and climate variability induced changes. LID features have the potential to mitigate impacts from large storm events, capturing, and recharging a significant quantity of freshwater that would alternatively discharge to the ocean. Additionally, this captured water has the potential to completely infiltrate over several days and ultimately become recharge. For coastal aquifer systems, this ability to redirect precipitation from runoff to recharge can potentially mitigate negative impacts from pumping and the inherent propensity for sea-water intrusion.

LID approaches can also potentially be used to capture excess runoff produced during El Niño years, providing excess recharge during drought years. For the grass lawn, recharge remained unchanged even under different precipitation scenarios because of the lack of runoff and ponding. ENSO precipitation intensities were predicted to change over the next century, and while this may cause an increase in overflow, this also leads to an increase in recharge because of the overall larger volumes entering the trench.

8.0 Acknowledgments

I would like to acknowledge the support from the G.A. Harris Research Instrumentation Grant from Decagon Devices for providing the equipment necessary to conduct this project. I also would like to thank the Geological Society of America for the research grant providing the funding for the Hydrus-3D purchase. Additionally, I would also like to acknowledge the efforts of Joshua Benton for help with Hydrus. I also acknowledge the efforts of the undergraduate field crew for helping me take daily water volume and waterlevel samples.

9.0 References

- Alpha Analytical Labs (2012), Alpha Analytical, [online] Available from:
<http://www.alphalab.com/> (Accessed 23 March 2012)
- Los Angeles and San Gabriel Rivers Watershed Council (2000), LA Basin Water Augmentation Study, [online] Available from:
https://wiki.epa.gov/watershed2/index.php/LA_Basin_Water_Augmentation_Study (Accessed 5 May 2012)
- Barbu, I. A., T. P. Ballestero, and R. M. Roseen (2008), LID-SWM Practices as a Means of Resilience to Climate Change and its Effects on Groundwater Recharge, in *Groundwater Resources Management: Adaptation Measures to Water Scarcity Science and Policy Responses*, p. 13, UNESCO, University of California Irvine.
- Bouwer, H., and R. C. Rice (1984), Hydraulic Properties of Stony Vadose Zones, *Ground Water*, 22(6).
- Bruce, B., D. Allen, H. Chaves, G. Grant, G. O. Essink, H. Kooi, I. White, J. Gurdak, J. Famiglietti, and J. L. Martin-Bordes (2008), Groundwater Resources Assessment under the Pressures of Humanity and Climate Changes, *United Nations Educational, Scientific and Cultural Organization (UNESCO)*, 32.
- California Department of Water Resources (2000), A Guide to Estimating Irrigation Water Needs of Landscape Plantings in California. The Landscape Coefficient Method and WUCOLS III, [online] Available from: <http://www.water.ca.gov/wateruseefficiency/docs/wucols00.pdf> (Accessed 15 April 2012)
- Cayan, D., R. Webb, H. F. Diaz, and V. Markgraf (1992), El Niño Southern Oscillation and streamflow in the western United States, in *El Niño: historical and paleoclimatic aspects of the southern oscillation*, pp. 29–68, Cambridge University Press, New York.
- City of Fresno (2012), Fresno's Groundwater Recharge Program, [online] Available from:
<http://www.fresno.gov/government/departmentsdirectory/publicutilities/watermanagement/groundwaterrecharg.htm> (Accessed 5 May 2012)

- Clifton, H. E., R. E. Hunter, and J. V. Gardner (1988), Analysis of Eustatic, Tectonic, and Sedimentologic Influences on Transgressive and Regressive Cycles in the Upper Cenozoic Merced Formation, San Francisco, California, in *New Perspectives in Basin Analysis*, edited by K. L. Kleinspehn and C. Paola, pp. 109–128, Springer-Verlag, New York.
- Crawley, M. J. (2007), *The R Book*, John Wiley, & Sons, Ltd, Chichester, Imperial College London at Silwood Park, UK.
- Davis, A. P. (2008), Field performance of bioretention: Hydrology impacts, *Journal of Hydrologic Engineering*, 13, 90.
- Davis, A. P., W. F. Hunt, R. G. Traver, and M. Clar (2009), Bioretention Technology: Overview of Current Practice and Future Needs, *Journal of Environmental Engineering*, 135(3), 109–117, doi:10.1061/(ASCE)0733-9372(2009)135:3(109).
- Decagon Devices (2012), Decagon Devices Products, [online] Available from: <http://www.decagon.com/products>
- Department of Environmental Resources (1999), *Low-Impact Development Hydrologic Analysis*, Department of Environmental Resources, Programs and Planning Division, Prince George's County, Maryland. [online] Available from: http://www.lowimpactdevelopment.org/pubs/LID_Hydrology_National_Manual.pdf (Accessed 2 September 2011)
- Department of Environmental Resources (2007), *Bioretention Manual*, Manual, Environmental Services Division, Department of Environmental Resources, Prince George's County, Maryland. [online] Available from: http://www.princegeorgescountymd.gov/Government/AgencyIndex/DER/ESG/Bioretention/pdf/Bioretention%20Manual_2009%20Version.pdf
- Dettinger, M. D., and D. R. Cayan (1994), Large-scale atmospheric forcing of recent trends toward early snowmelt runoff in California, *Journal of Climate*, 8, 606–624.
- Dettinger, M. D., D. S. Battisti, R. D. Garreaud, G. J. McCabe, and C. M. Bitz (2001), Interhemispheric effects of interannual and decadal ENSO-like climate variations on the Americas, in *Present and Past Interhemispheric Climate Linkages in the Americas and their Societal Effects*, pp. 1–16.

- Dietz, M. E. (2005), Rain Garden Design and Function: A Field Monitoring and Computer Modeling Approach, Dissertation, University of Connecticut, Connecticut.
- Dietz, M. E. (2007), Low Impact Development Practices: A Review of Current Research and Recommendations for Future Directions, *Water, Air, and Soil Pollution*, 186(1-4), 351–363, doi:10.1007/s11270-007-9484-z.
- Dietz, M. E., and J. C. Clausen (2005), A Field Evaluation of Rain Garden Flow and Pollutant Treatment, *Water, Air, and Soil Pollution*, 167(1-4), 123–138, doi:10.1007/s11270-005-8266-8.
- Dietz, M. E., and J. C. Clausen (2006), Saturation to Improve Pollutant Retention in a Rain Garden, *Environmental Science & Technology*, 40(4), 1335–1340, doi:10.1021/es051644f.
- Dietz, M. E., and J. C. Clausen (2008), Stormwater runoff and export changes with development in a traditional and low impact subdivision, *Journal of Environmental Management*, 87(4), 560–566, doi:16/j.jenvman.2007.03.026.
- Dingman, S. L. (2002), *Physical Hydrology*, Prentice-Hall, Inc., University of New Hampshire.
- Earman, S., and M. D. Dettinger (2011), Potential impacts of climate change on groundwater resources - a global review, *Journal of Water and Climate Change*, 2(4), 213–229.
- Endreny, T., and V. Collins (2009), Implications of bioretention basin spatial arrangements on stormwater recharge and groundwater mounding, *Ecological Engineering*, 35(5), 670–677, doi:10.1016/j.ecoleng.2008.10.017.
- Enfield, D. B., A. M. Mestas-Nunez, and P. J. Trimble (2001), The Atlantic Multidecadal Oscillation and its relationship to rainfall and river flows in the continental U.S., *Geophysical Research Letters*, 28, 2077–2080.
- Ermilio, J. R., and R. G. Traver (2006), Hydrologic and Pollutant Removal Performance of a Bio-Infiltration BMP, in *Proceedings of the World Environmental and Water Resources Congress*, vol. 200, pp. 394–394, ASCE. [online] Available from:

<http://link.aip.org/link/ASCECP/v200/i40856/p394/s1&Agg=doi>
(Accessed 25 March 2012)

- van Genuchten, M. T., F. J. Leij, and S. R. Yates (1991), *The RETC Code for Quantifying the Hydraulic Functions of Unsaturated Soils*, U.S. Salinity Laboratory, USDA, ARS, Riverside, California.
- Green, T. R., M. Taniguchi, and H. Kooi (2007), Potential impacts of climate change and human activity on subsurface water resources, *Vadose Zone Journal*, 6(3), 531.
- Green, T. R., M. Taniguchi, H. Kooi, J. J. Gurdak, D. Allen, H. Treidel, and A. Aureli (2011), Beneath the surface of global change: Impacts of climate change on groundwater, Invited review paper, *Journal of Hydrology*, 405, 532–560, doi:doi:10.1016/j.jhydrol2011.05.002.
- Gurdak, J. J., R. T. Hanson, P. B. McMahon, B. W. Bruce, J. E. McCray, G. D. Thyne, and R. C. Reedy (2007), Climate Variability Controls on Unsaturated Water and Chemical Movement, High Plains Aquifer, USA, *Vadose Zone Journal*, 6(3), 533–547, doi:10.2136/vzj2006.0087.
- Gurdak, J. J., R. T. Hanson, and T. R. Green (2009), *Effects of Climate Variability and Change on Groundwater Resources of the United States*, Effects of Climate Variability and Change on Groundwater Resources of the United States: U.S. Geological Survey Fact Sheet 2009-3074. [online] Available from: <http://pubs.usgs.gov/fs/2009/3074/> (Accessed 6 March 2012)
- Healy, R. W. (2010), *Estimating Groundwater Recharge*, Cambridge University Press.
- Helsel, D. R., and R. M. Hirsch (2002), *Statistical Methods in Water Resources*, Techniques of Water-Resources Investigations Book 4, U.S. Geological Survey. [online] Available from: <http://pubs.usgs.gov/twri/twri4a3/>
- Holman, I. P., M. Rivas-Casado, N. J. K. Howden, J. P. Bloomfield, and A. T. Williams (2009), Linking North Atlantic ocean - atmosphere teleconnection patterns and hydrogeological responses in temperate groundwater systems, *Hydrol. Process.*, 23, 2123–2126.
- Holman, I. P., M. Rivas-Casado, J. P. Bloomfield, and J. J. Gurdak (2011), Identifying non-stationary groundwater level response to North Atlantic

ocean-atmosphere teleconnection patterns using wavelet coherence, *Hydrogeol. J.*, 19(6), 1269–1278, doi:10.1007/s10040-011-0755-9.

HydroFocus Inc. (2012), HydroFocus, Inc. - Evaluation of Westside Basin Groundwater Resources and Quality, [online] Available from: <http://www.hydrofocus.com/westside.html> (Accessed 8 April 2012)

IPCC (2007), *Climate change 2007: synthesis report. Contribution of Working Groups I, II and III to the Fourth Assessment Report of the Intergovernmental Panel on Climate Change*, Intergovernmental Panel on Climate Change, Geneva.

Kay, A. L., and H. N. Davies (2008), Calculating potential evaporation from climate model data: A source of uncertainty for hydrological climate change impacts, *Journal of Hydrology*, 358(3-4), 221–239, doi:10.1016/j.jhydrol.2008.06.005.

Labat, D. (2008), Wavelet analysis of the annual discharge records of the world's largest rivers, *Advances in Water Resources*, 31(1), 109–117, doi:10.1016/j.advwatres.2007.07.004.

Laws, B. V., E. R. V. Dickenson, T. A. Johnson, S. A. Snyder, and J. E. Drewes (2011), Attenuation of contaminants of emerging concern during surface-spreading aquifer recharge, *Science of The Total Environment*, 409(6), 1087–1094, doi:10.1016/j.scitotenv.2010.11.021.

Lerner, D. (2002), Identifying and quantifying urban recharge: a review, *Hydrogeology Journal*, 10(1), 143–152, doi:10.1007/s10040-001-0177-1.

Lerner, D. N. (1990), Groundwater recharge in urban areas, *Atmospheric Environment. Part B. Urban Atmosphere*, 24(1), 29–33, doi:10.1016/0957-1272(90)90006-G.

Maimone, M., D. E. O'Rourke, J. O. Knighton, and C. P. Thomas (2011), Potential Impacts of Extensive Stormwater Infiltration in Philadelphia, *Environmental Engineer: Applied Research and Practice*, 14(Fall).

McCabe, G. J., M. A. Palecki, and J. L. Betancourt (2004), Pacific and Atlantic Ocean influences on multidecadal drought frequency in the United States, in *Proceedings of the National Academy of Sciences*, vol. 101, pp. 4136–4141.

- McMahon, P. B., K. F. Dennehy, R. L. Michel, M. A. Sophocleous, K. . Ellett, and D. B. Hurlbut (2003), *Water Movement Through Thick Unsaturated Zones Overlying the Central High Plains Aquifer, Southwestern Kansas, 2000-2001*, Water-Resources Investigations Report 03-4171, U.S. Geological Survey.
- McMahon, P. B., L. N. Plummer, J. K. Böhlke, S. D. Shapiro, and S. R. Hinkle (2011), A comparison of recharge rates in aquifers of the United States based on groundwater-age data, *Hydrogeol. J.*, doi:10.1007/s10040-011-0722-5.
- Miller, M. (2006), Rainwater Harvesting for Enhanced Groundwater Recharge Through Capture of Increased Runoff from Site Development, OpenSIUC, Southern Illinois University Carbondale.
- Miller, N. L. (2003), *California Climate Change, Hydrologic Response, and Flood Forecasting*, International Expert Meeting on Urban Flood Management, Earth Sciences Division, Berkeley National Laboratory, World Trade Center Rotterdam, The Netherlands.
- Mishra, V., and D. P. Lettenmaier (2011), Climatic trends in major U.S. urban areas, 1950–2009, *Geophysical Research Letters*, 38(16), doi:10.1029/2011GL048255. [online] Available from: <http://www.agu.org/pubs/crossref/2011/2011GL048255.shtml> (Accessed 23 January 2012)
- Natural Resources Conservation Service (1986), *Urban Hydrology for Small Watersheds*, Technical Manual, United States Department of Agriculture-Conservation Engineering Division.
- NOAA (2012), Climate Timeseries, *GCOS Working Group on Surface Pressure*. [online] Available from: http://www.esrl.noaa.gov/psd/gcos_wgsp/Timeseries/ (Accessed 18 April 2012)
- NOAA ESRL (2012), MEI timeseries from Dec/Jan 1940/50 up to the present, [online] Available from: <http://www.esrl.noaa.gov/psd/enso/mei/table.html> (Accessed 18 April 2012)

- NOAA GFDL (2012), Geophysical Fluid Dynamics Laboratory - Welcome to GFDL, *Geophysical Fluid Dynamics Laboratory*. [online] Available from: <http://www.gfdl.noaa.gov/> (Accessed 13 March 2012)
- NOAA NCDC (2011), NCDC National Climatic Data Center (NCDC), [online] Available from: <http://www.ncdc.noaa.gov/oa/ncdc.html> (Accessed 3 June 2011)
- Nzewi, O., J. A. Gilman, and G. Bartow (2010), *2009 Annual Groundwater Monitoring Report, Westside Basin*, San Francisco Public Utilities Commission. [online] Available from: <http://sfwater.org> (Accessed 29 August 2010)
- PC-Progress (2011), PC-PROGRESS - Homepage, *PC-Progress Engineering Software Developer*. [online] Available from: <http://www.pc-progress.com/en/Default.aspx> (Accessed 13 January 2012)
- Phillips, S. P., S. N. Hamlin, and E. B. Yates (1993), *Geohydrology, Water Quality, and Estimation of Ground-Water Recharge in San Francisco, California, 1987-1992*, WRIR 93-4019, U.S. Geological Survey.
- Pierce, D. W. et al. (2012), Probabilistic estimates of future changes in California temperature and precipitation using statistical and dynamical downscaling, *Climate Dynamics*, doi:10.1007/s00382-012-1337-9. [online] Available from: <http://www.springerlink.com/index/10.1007/s00382-012-1337-9> (Accessed 6 May 2012)
- Pitt, R. (1999), Small storm hydrology and why it is important for the design of stormwater control practices., in *Advances in modeling the management of stormwater impacts*, vol. 7, edited by W. James, Computational Hydraulics International and Lewis Publishers/CRC Press, Guelph, Ontario.
- Pyke, C., M. P. Warren, T. Johnson, J. LaGro Jr., J. Scharfenberg, P. Groth, R. Freed, W. Schroerer, and E. Main (2011), Assessment of low impact development for managing stormwater with changing precipitation due to climate change, *Landscape and Urban Planning*, 103(2), 166–173, doi:10.1016/j.landurbplan.2011.07.006.
- Richards, L. . (1931), Capillary conduction of liquids in porous mediums, *Physics*, 1, 318–333.

- Romero, C. C., and M. D. Dukes (2009), Turfgrass and Ornamental Plant Evapotranspiration and Crop Coefficient Literature Review,
- Roy-Poirier, A., P. Champagne, and Y. Fillion (2010), Review of Bioretention System Research and Design: Past, Present, and Future, *Journal of Environmental Engineering*, 136(9), 878–889, doi:10.1061/(ASCE)EE.1943-7870.0000227.
- Scanlon, B. R., R. W. Healy, and P. G. Cook (2002), Choosing appropriate techniques for quantifying groundwater recharge, *Hydrogeol. J.*, 10, 18–39.
- Schlea, D. A. (2011), Retention and management of stormwater runoff with rain gardens and rainwater harvesting systems, Ohio State University, Graduate Program in Food, Agricultural, and Biological Engineering.
- SFPUC (2012), San Francisco Public Utilities Commission : Urban Watershed Planning, [online] Available from: <http://sfwater.org/index.aspx?page=460> (Accessed 5 May 2012)
- SFPUC and Wastewater Enterprise (2009), Low-Impact Design in San Francisco-LID Technical Workshop, [online] Available from: <http://sfwater.org/index.aspx?page=314>
- Shang, H., J. Yan, and X. Zhang (2011), El Niño–Southern Oscillation influence on winter maximum daily precipitation in California in a spatial model, *Water Resources Research*, 47(11), doi:10.1029/2011WR010415. [online] Available from: <http://www.agu.org/pubs/crossref/2011/2011WR010415.shtml> (Accessed 29 December 2011)
- Shuster, W. D., R. Gehring, and J. Gerken (2007), Prospects for enhanced groundwater recharge via infiltration of urban storm water runoff: A case study, *Journal of Soil and Water Conservation*, 62(3), 129–136.
- Simunek, J., M. T. van Genuchten, and M. Sejna (2008), Development and Applications of the HYDRUS and STANMOD Software Packages and Related Codes, *Vadose Zone Journal*, 7(2), 587–600, doi:10.2136/vzj2007.0077.
- Solinst Inc. (2011), Levellogger User Guide,

- Stephens, D. B., M. Miller, S. J. Moore, T. Umstot, and D. J. Salvato (2012), Decentralized Groundwater Recharge Systems Using Roofwater and Stormwater Runoff, *JAWRA Journal of the American Water Resources Association*, 48(1), 134–144, doi:10.1111/j.1752-1688.2011.00600.x.
- Taylor, R., and C. Tindimugaya (2012), The impacts of climate change and rapid development on weathered crystalline rock aquifer systems in the humid tropics of sub-Saharan Africa: evidence from south-western Uganda, in *Climate change effects on groundwater resources: A global synthesis of findings and recommendations*, International Association of Hydrogeologists (IAH) - International Contributions to Hydrogeology, edited by H. Treidel, J. L. Martin-Bordes, and J. J. Gurdak, Taylor & Francis Publishing.
- The Irrigation Association (2010), Landscape Irrigation Auditor,
- Treidel, H., J. L. Martin-Bordes, and J. J. Gurdak (Eds.) (2012), *Climate change effects on groundwater resources: A global synthesis of findings and recommendations*, International Association of Hydrogeologists (IAH) - International Contributions to Hydrogeology, Taylor & Francis Publishing.
- Tremblay, L., M. Larocque, F. Anctil, and C. Rivard (2011), Teleconnections and interannual variability in Canadian groundwater levels, *Journal of Hydrology*, 410(3-4), 178–188, doi:10.1016/j.jhydrol.2011.09.013.
- UNESCO (2008), *Groundwater resources assessment under the pressures of humanity and climate change (GRAPHIC) – A framework document*, United Nations Educational, Scientific and Cultural Organization (UNESCO) Publications, Paris, France. [online] Available from: http://www.unesco.org/water/ihp/graphic/media/GRAPHIC_Series_No2_WEB.pdf
- US EPA (2000), *Low impact development (LID), a literature review.*, United States Environmental Protection Agency.
- Vicente-Serrano, S. M., J. I. López-Moreno, L. Gimeno, R. Nieto, E. Morán-Tejeda, J. Lorenzo-Lacruz, S. Beguería, and C. Azorin-Molina (2011), A multiscale global evaluation of the impact of ENSO on droughts, *J. Geophys. Res.*, 116(D20), doi:10.1029/2011JD016039. [online] Available from: <http://www.agu.org/pubs/crossref/2011/2011JD016039.shtml> (Accessed 5 April 2012)

- Wang, C., C. Deser, J.-Y. Yu, P. DiNezio, and A. Clement (2012), El Niño and Southern Oscillation (ENSO): A Review, in *Coral Reefs of the Eastern Pacific*, Springer.
- Wolter, K., and M. S. Timlin (1993), Monitoring ENSO in COADS with a seasonally adjusted principal component index, in *Proc. of the 17th Climate Diagnostics Workshop*, pp. 52–57, NOAA/NMC/CAC, NSSL, Oklahoma Clim. Survey, CIMMS and the School of Meteor., Univ. of Oklahoma, Norman,, OK.
- Wolter, K., and M. S. Timlin (1998), Measuring the strength of ENSO events- How does 1997/1998 rank?, *Weather*, 53(9), 315–324.
- WRCC (2012), Western Regional Climate Center, [online] Available from: <http://www.wrcc.dri.edu/> (Accessed 24 March 2012)
- Yeh, S.-W., B. P. Kirtman, J.-S. Kug, W. Park, and M. Latif (2011), Natural variability of the central Pacific El Nino event on multi-centennial timescales, *J. Geophys. Res.*, 38(L02704), doi:10.1029/2010GL045886.

10.0 Figures and Tables

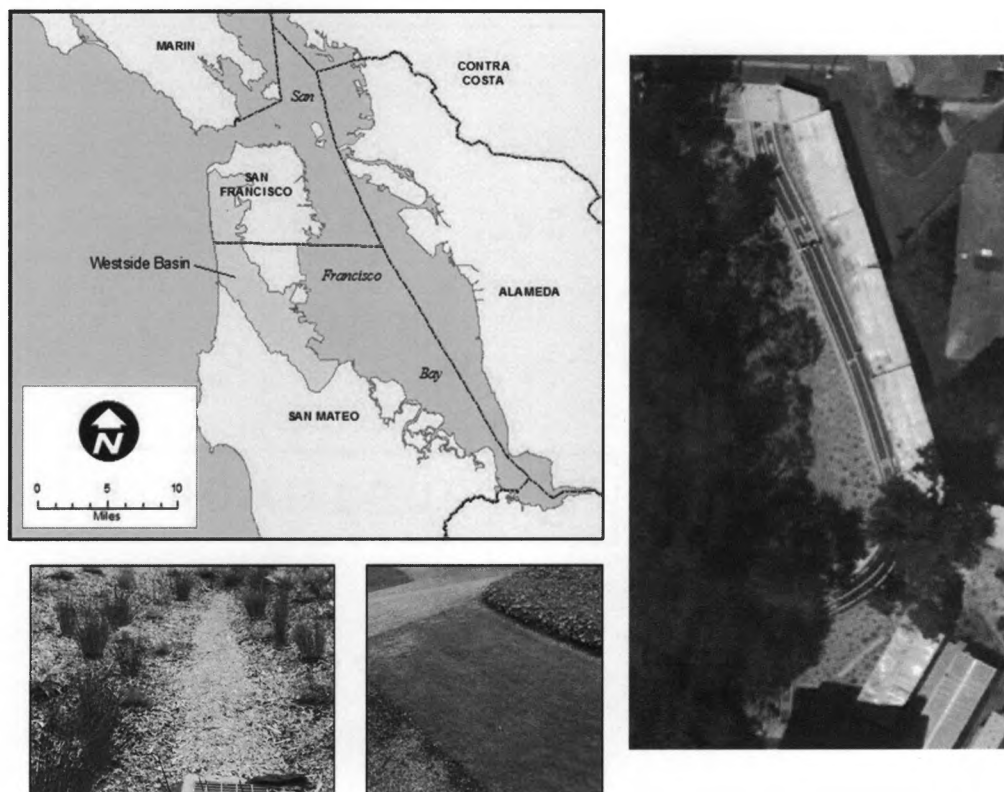


Figure 1: The Westside Basin aquifer located on the San Francisco Peninsula, CA. The infiltration trench is shown in the top right photo and the grass lawn in the lower right. Map credit to [HydroFocus Inc., 2012].

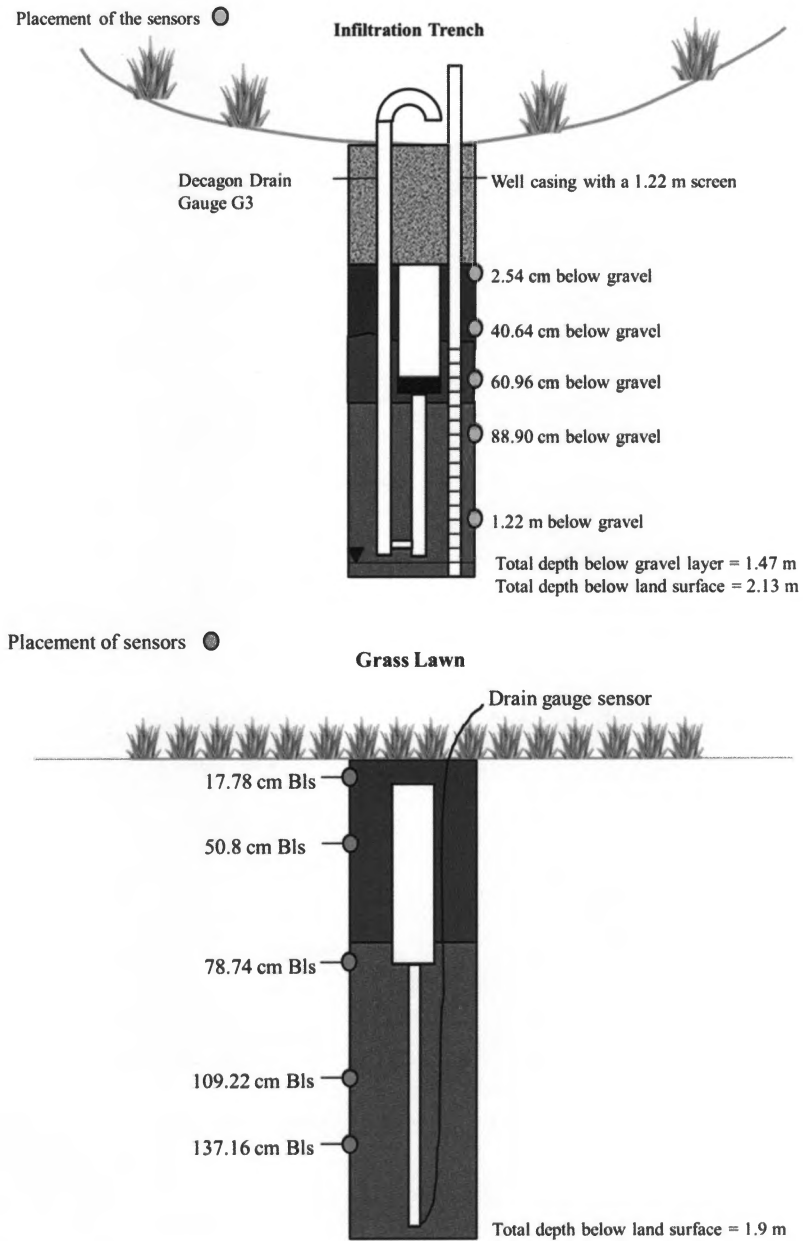


Figure 2: Instrumentation setup for the infiltration trench (top) and the irrigated grass lawn (bottom). Green dots show the locations of the water content and matric potential sensors throughout the soil column.

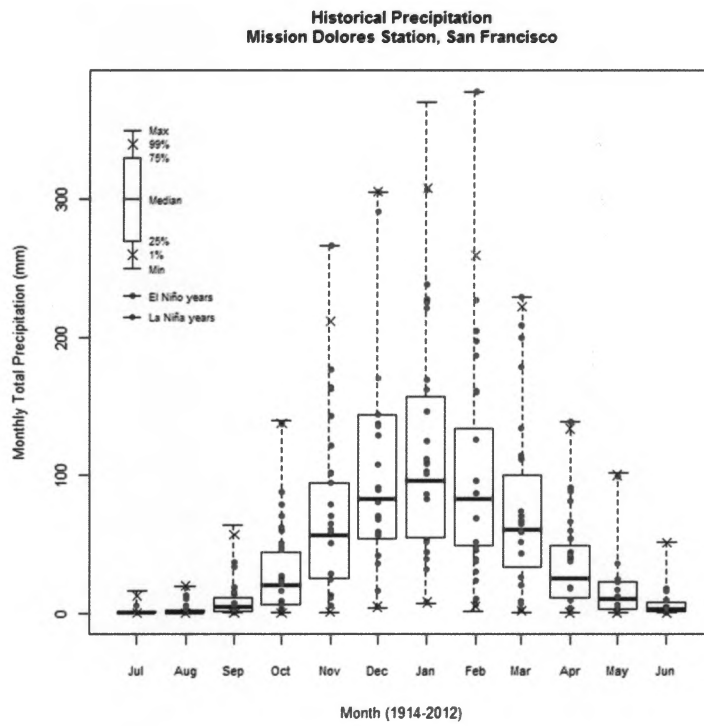


Figure 3: Historical monthly precipitation distribution for the study site.

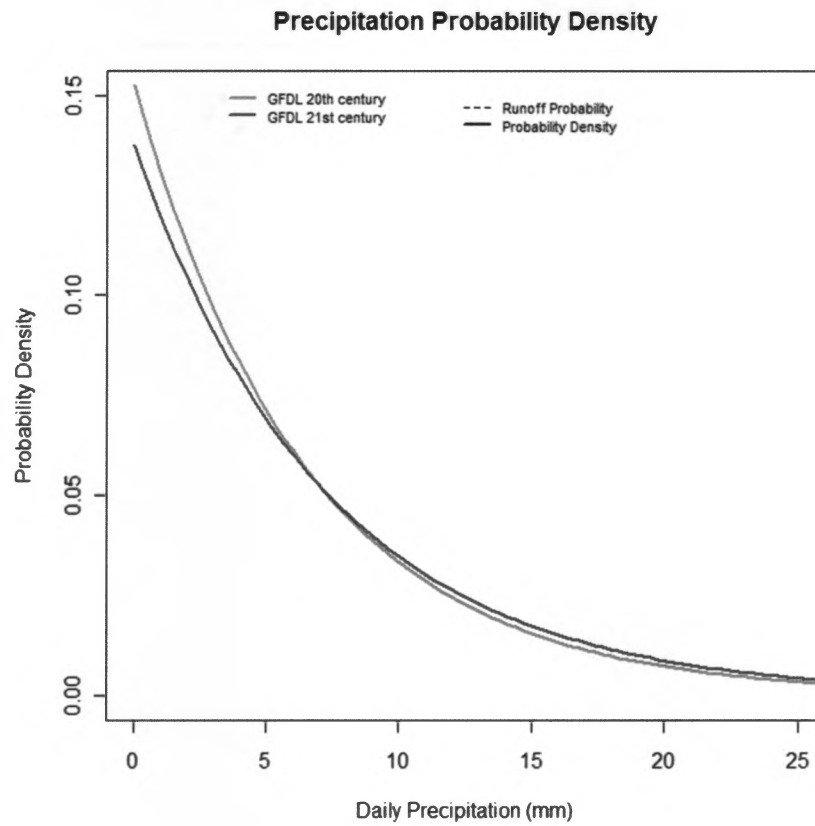


Figure 4: Modeled historical GFDL20th century and forecasted GFDL 21st century future daily precipitation probability densities.

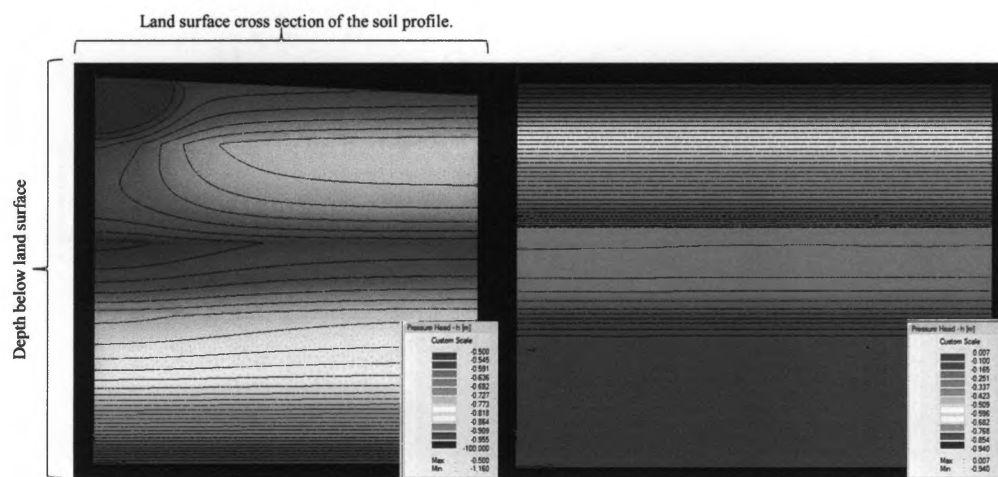


Figure 5: Hydrus-2D model domain for the irrigated grass lawn (left) and the infiltration trench (right). Pressure heads (L) associated with each color are shown in the figure legends.

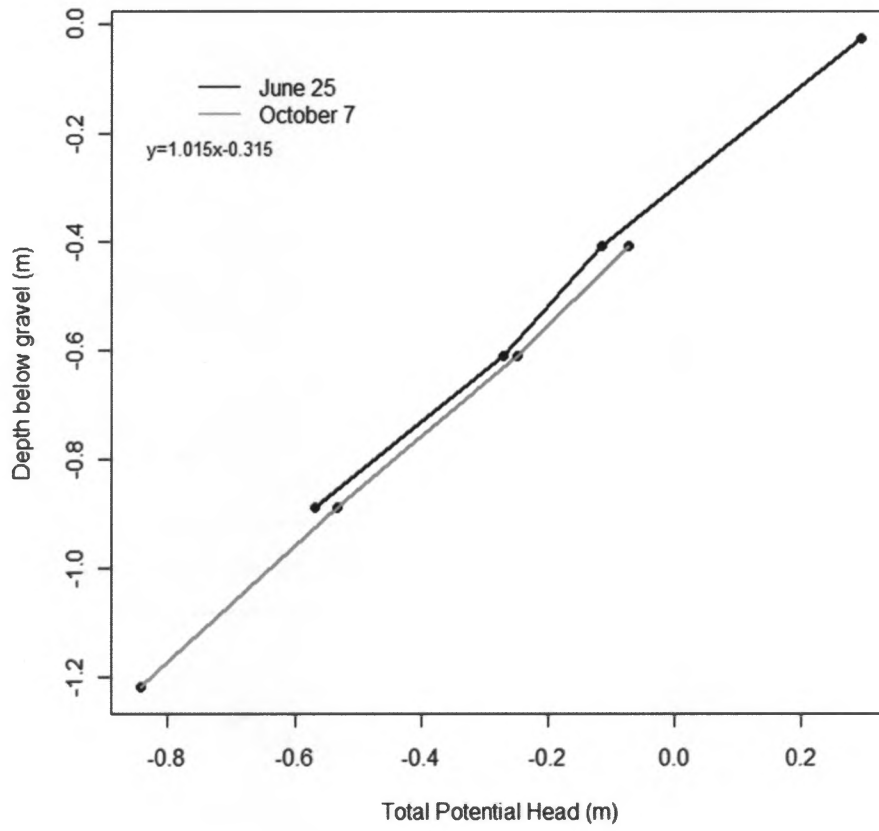


Figure 6: Infiltration trench total potential profiles.

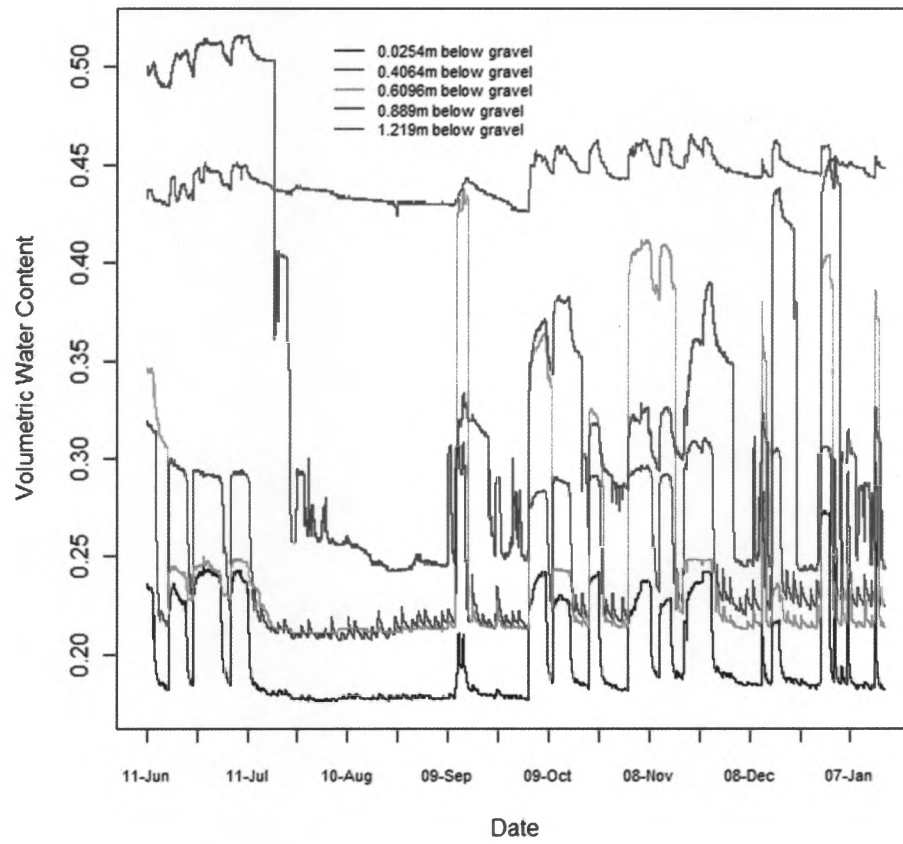


Figure 7: Infiltration trench water content during the summer and fall 2011, and spring 2012.

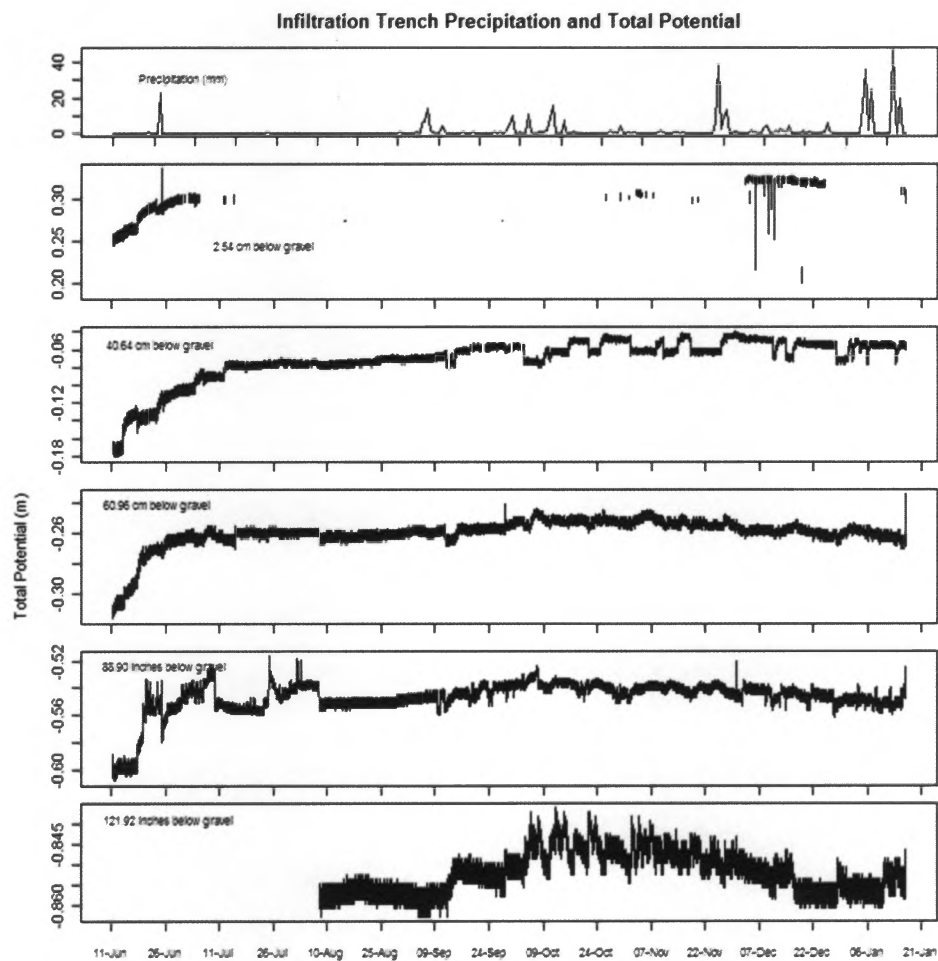


Figure 8: Infiltration trench total potentials during the summer and fall 2011.

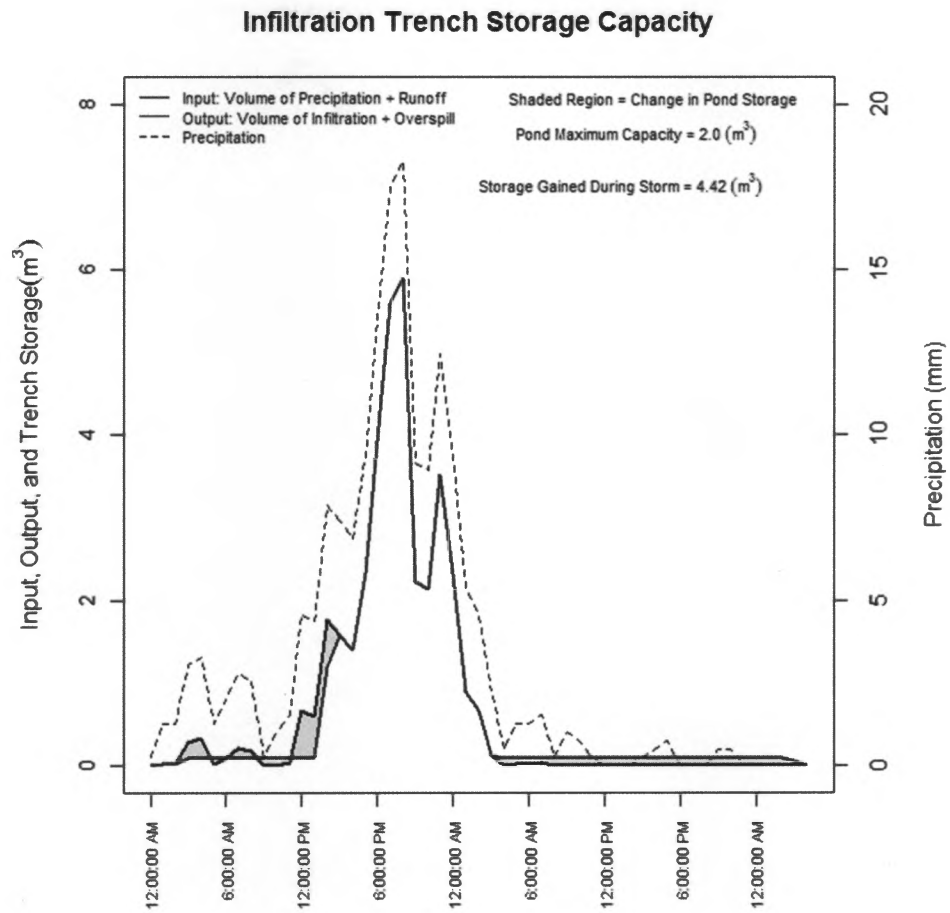


Figure 9: Trench storage capacity during the largest recorded storm. Over 140 mm of precipitation occurred in just one day and over 170 mm over 2 days.

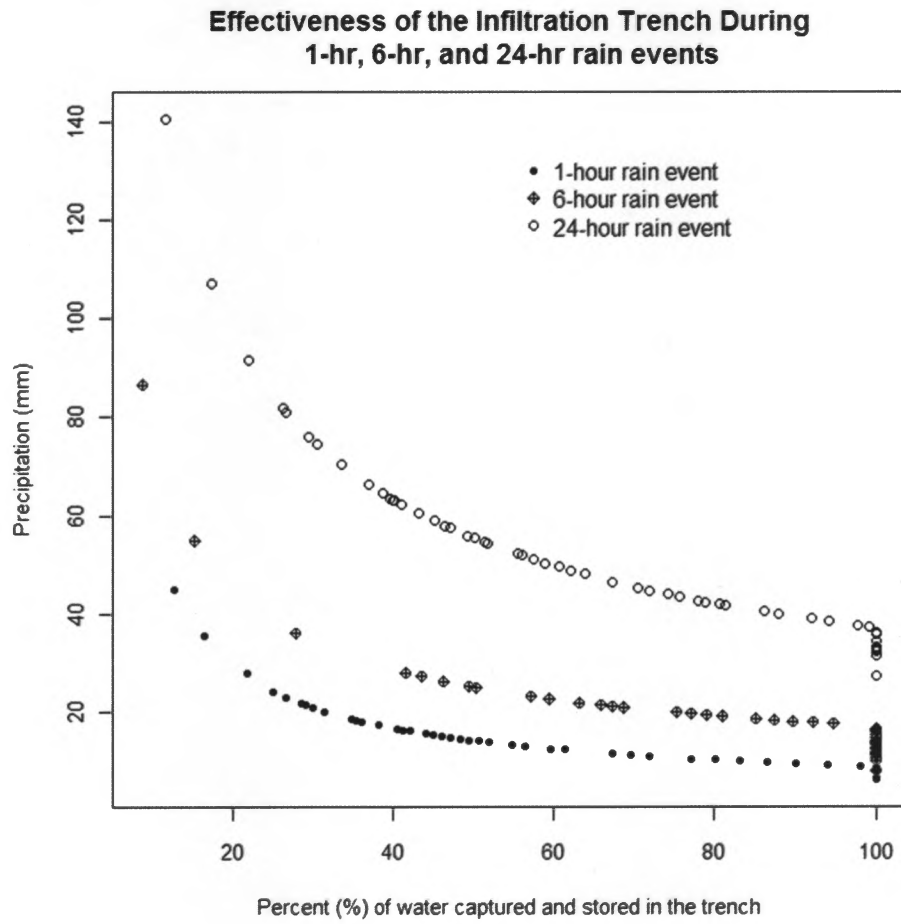


Figure 10: Percent of water capture and stored by the gravel in the infiltration trench is shown and is separated by the magnitude of the rain event.

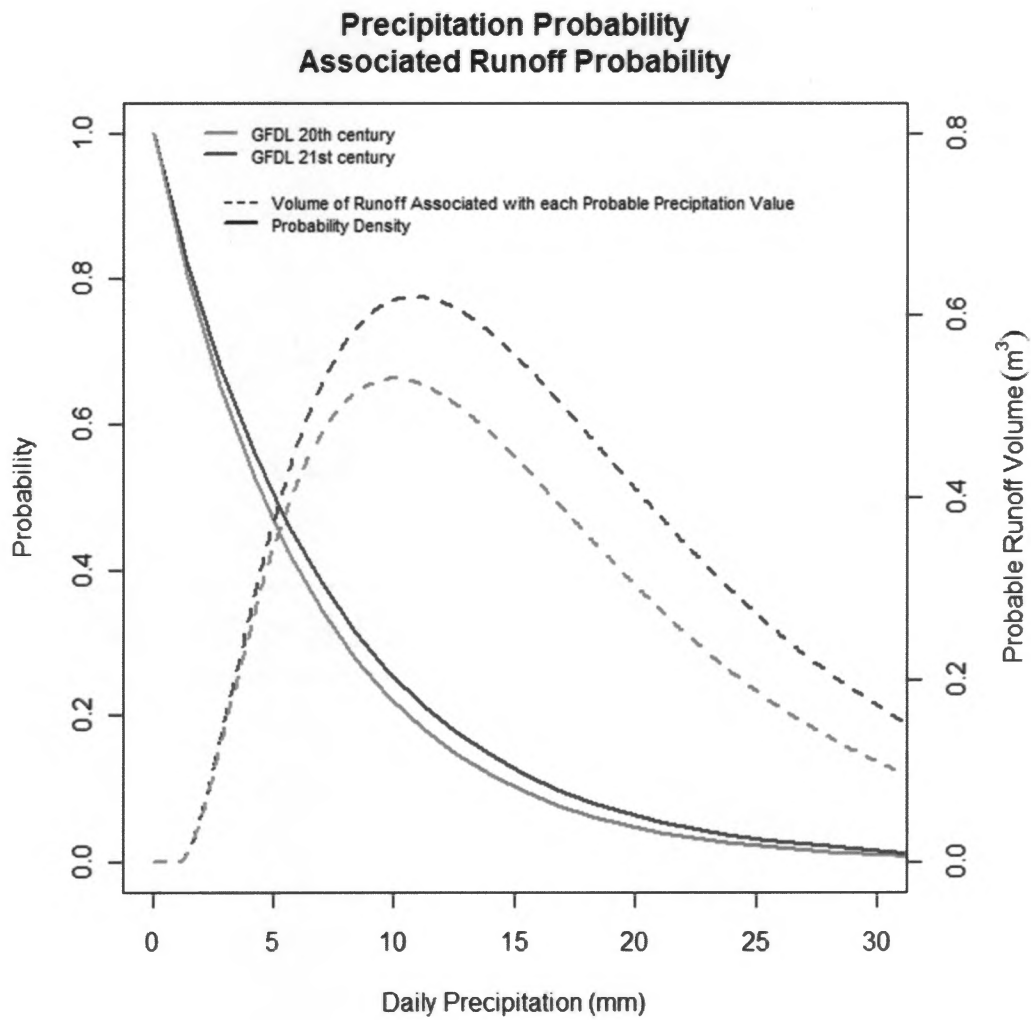


Figure 11: Probability distributions of yearly historical and future precipitation events and the associated runoff probability distributions from the precipitation probabilities.

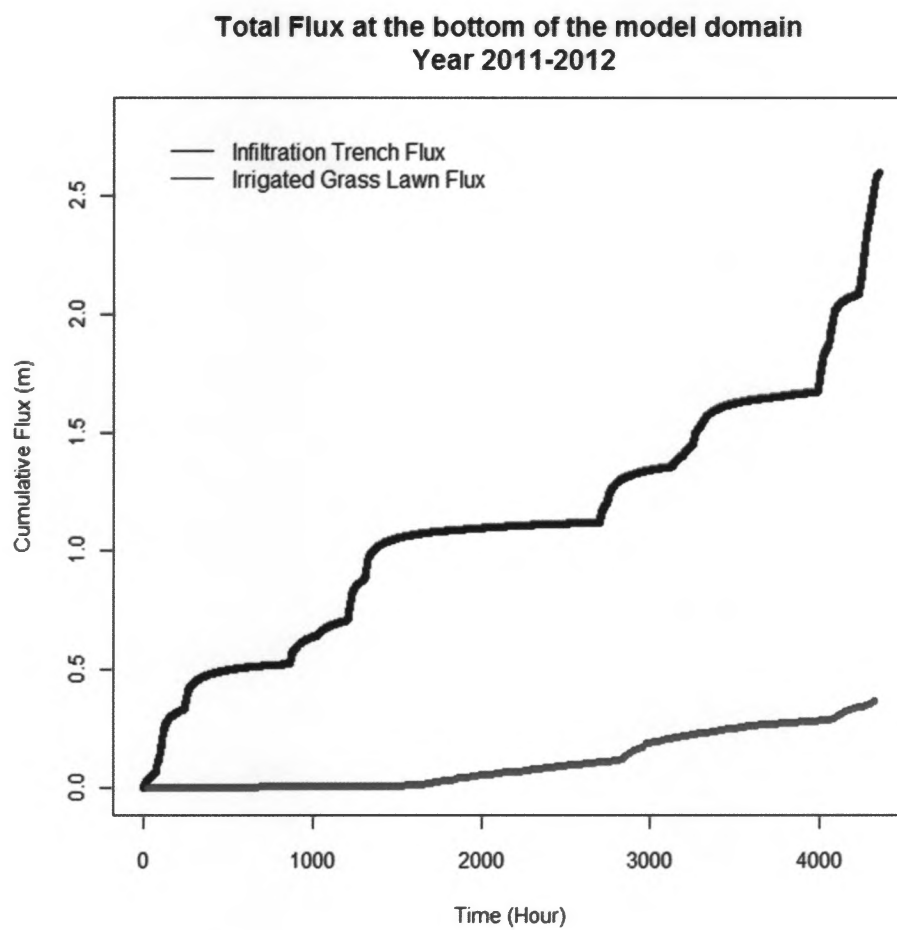


Figure 12: Cumulative flux at the free-drainage boundary of the Hydrus-2D model domain.

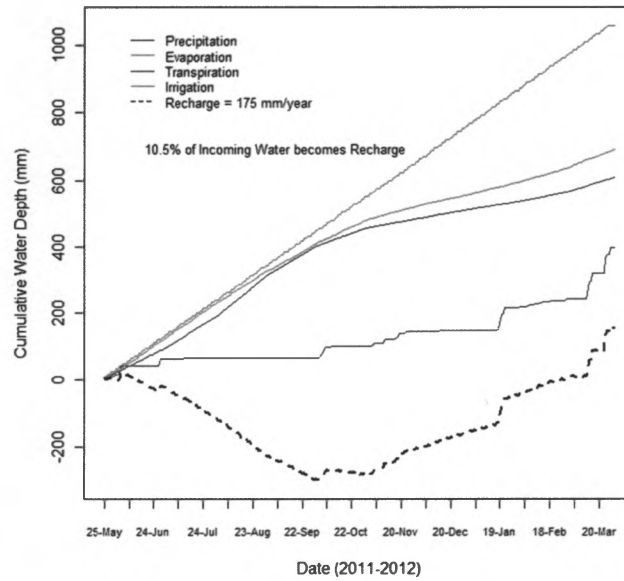
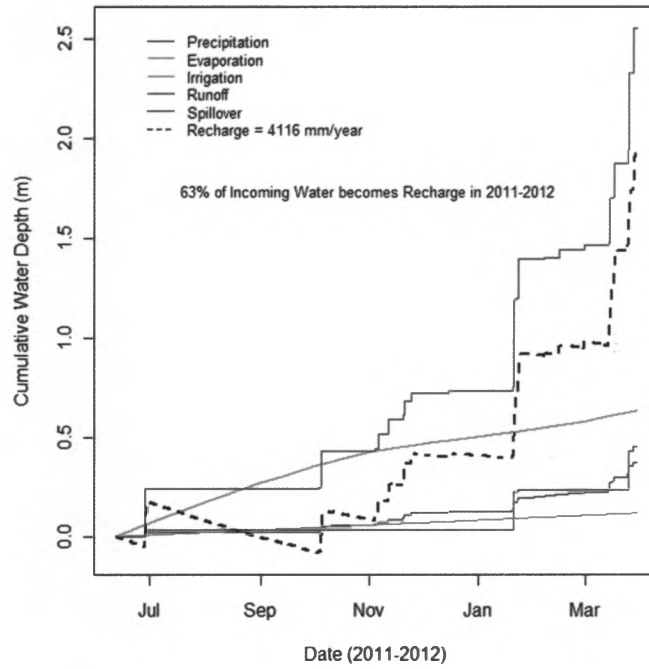


Figure 13: Water budget for the infiltration trench (top) and the grass lawn (bottom).

Table 1: Rain depths associated with different probability return intervals.

Return Period	Rain Depth (mm)		
	1-hr	6-hr	24-hr
2 years	13.21	17.78	45.20
5 years	17.27	21.84	63.00
10 years	21.34	25.15	74.40
25 years	27.94	36.07	91.70
50 years	43.96	85.31	138.51

Table 2: van Genuchten parameters for the irrigated turf grass lawn.

Grassy Lawn			Depth	θ_r	θ_s	α	n	l	K_s
Sand-Silt-Clay	% Gravel by Mass	Soil Type	(m)	(-)	(-)	(m^{-1})	(-)	(m^{-1})	(m/day)
86-2-11	22.6	Loamy Sand	0-0.178	0.046	0.294	2.920	1.941	0.5	1.040
88-2-9	1	Loamy Sand	0.178-0.508	0.052	0.310	3.180	1.957	0.5	0.857
88-2-9	0.4	Loamy Sand	0.508-.788	0.055	0.354	3.080	2.082	0.5	1.531
88-2-9	0.2	Loamy Sand	0.788-1.092	0.055	0.351	3.090	2.069	0.5	1.473
92-2-5	1.2	Sand	1.092-1.372	0.051	0.336	3.240	2.628	0.5	3.007

Table 3: van Genuchten parameters for the LID infiltration trench.

Infiltration trench			Depth	θ_r	θ_s	α	n	l	K_s
Sand-Silt-Clay	% Gravel by Mass	Soil Type	(m)	(-)	(-)	(m^{-1})	(-)	(m^{-1})	(m/day)
0-0-0	100	Pure Gravel	0-1.000	0.000	0.510	10.95	1.722	0.5	84000
76-8-15	86.5	Mixed Gravel	1.000-1.060	0.021	0.145	2.989	1.461	0.5	0.154
86-2-11	0.3	Loamy Sand	0-1.060	0.061	0.399	2.880	1.991	0.5	1.666
84-4-11	0.8	Loamy Sand	1.060-1.270	0.053	0.344	3.240	1.737	0.5	0.726
64-8-27	8.6	Sandy Clay Loam	1.270-1.549	0.055	0.320	2.990	1.209	0.5	0.072
64-8-27	19.5	Sandy Clay Loam	1.549-1.880	0.050	0.287	2.920	1.217	0.5	0.071

Table 4: Summary statistics for hourly and daily data from the Mission Dolores station, SF.

Data Type	Hourly data	Data Type	Daily data
Time Frame	1948-2011	Time Frame	1914-2012
COOPID	47772	COOPID	47772
Station: Mission Dolores, SF		Station: Mission Dolores, SF	
Source:		Source:	
http://www.ncdc.noaa.gov/		http://www.wrcc.dri.edu/	
	<u>mm/hour</u>		<u>mm/day</u>
Mean	1.353	Mean	10.900
Standard Error	0.774	Standard Error	7.250
Median	0.760	Median	7.942
Mode	0.254	Mode	0.300
Standard Deviation	1.730	Standard Deviation	10.250
1st percentile	0.250	1st percentile	0.300
25th percentile	0.254	25th percentile	1.000
75th percentile	1.778	75th percentile	10.900
99th percentile	8.128	99th percentile	46.610
Sample Variance	2.995	Sample Variance	105.128
Kurtosis	46.424	Kurtosis	15.569
Skewness	4.368	Skewness	2.698
Range	44.710	Range	140.400
Minimum	0.250	Minimum	0.300
Maximum	44.960	Maximum	140.700
# of records	102,480	# of records	6,646

Table 5: Daily percent change averaged by month under the GFDL A1F1 scenario.

	Jan	Feb	Mar	Apr	May	June	July	Aug	Sept	Oct	Nov	Dec
Historical (1861-2000)	9.55	8.77	5.58	3.57	2.17	1.26	2.03	2.38	4.11	4.53	6.17	8.80
Predicted (2000-2100)	11.84	9.03	6.20	2.68	1.94	1.42	1.03	1.89	3.78	4.69	5.31	8.53
Percent Change	+23.9%	+2.9%	+11.1%	-24.9%	-10.6%	+12.1%	-49.3%	-20.6%	-8.0%	+3.4%	-13.9%	-3.1%
χ^2	74.39	1.02	0.12	190.71	149.88	151.91	1673.04	501.90	60.71	3.80	145.34	17.65
d.f.	1	1	1	1	1	1	1	1	1	1	1	1
p	< 0.01	0.31	0.73	< 0.01	< 0.01	< 0.01	< 0.01	< 0.01	< 0.01	0.05	< 0.01	< 0.01

Table 6: Daily intensity percent change under the GFDL A1F1 scenario.

	Low (< 8 mm)	High (> 8 mm)
Historical (1861-2000)	2.18	18.85
Predicted (2000-2100)	2.11	20.96
Percent Change	-3.2%	+11.2%
χ^2	3.87	30.92
d.f.	1	1
p	0.04	< 0.01

Table 7: Recharge calculated for the 2011-2012 water year for the infiltration trench and grass lawn.

Recharge				
Method	Infiltration Trench (mm/year)	Infiltration Trench (m ³ /year)	Grass Lawn (mm/year)	*Grass Lawn (m ³ /year)
Water Budget	1,955	21	175	75
1D-Darcy	2,344	25	511	220
In-situ Drainage	1,623	18	130	56
Hydrus-2D (2011-2012)	2,582	28	409	176
Hydrus-2D (2099-2100)	3,714	40	726	312
Recharge Probability	5,111	55	170	73

* The area for the grass lawn is based on a hypothetical scenario where the grass lawn has an equivalent natural area of 430 m² which is the effective area contributing to the BMP site

Table 8: Recharge calculated from the probability analysis for the different precipitation scenarios in the infiltration trench.

Infiltration Trench					
Volume of Total Runoff Infiltrated and Recharged-Yearly Probability Analysis					
	Volume Runoff from the bike path (m³)	Precipitation Volume falling on the trench(m³)	Irrigation Volume (m³)	Volume Recharged (m³)	Recharge (m/year)
Historical					
2011-2012	157.29	6.68	1.24	55.18	5.11
Average Historical	162.11	6.81	1.24	56.84	5.26
Historical El Niño	207.20	8.36	1.24	72.41	6.70
Historical La Niña	137.71	5.96	1.24	48.40	4.48
GFDL Simulated					
Simulated GFDL A1F1	165.28	6.93	1.24	57.93	5.36
Simulated A1F1 El Niño	210.04	8.46	1.24	73.39	6.80
Simulated A1F1 La Niña	139.86	6.03	1.24	49.14	4.55

Table 9: Recharge calculated from the probability analysis for the seven different historical and predicted precipitation scenarios in the grass lawn.

Grass Lawn				
Volume of Total Runoff Infiltrated and Recharged-Yearly Probability Analysis				
Historical	Precipitation Volume (m³)	Irrigation Volume (m³)	Volume Recharged (m³)	Recharge (m/year)
2011-2012	2.47	4.04	0.68	0.17
Average Historical	2.52	4.04	0.68	0.17
Historical El Niño	3.10	4.04	0.74	0.19
Historical La Niña	2.21	4.04	0.65	0.16
GFDL Simulated				
Simulated GFDL A1F1	2.56	4.04	0.69	0.17
Simulated A1F1 El Niño	3.13	4.04	0.75	0.19
Simulated A1F1 La Niña	2.23	4.04	0.65	0.16

11.0 Chapter 3—Supporting Information

11.1 Experimental Field Set-up

The maximum drainage area to the infiltration trench is shown in Figure 14. Piezometers were installed at three locations within the infiltration trench. The piezometers were installed at the base of the gravel layer to determine the water level within the infiltration trench on a daily basis using pressure transducers located inside each piezometer. Each piezometer was constructed of pvc pipe with a slotted screen and extended to 25 cm above the gravel layer. The locations of the piezometers and a cross-section of the infiltration trench is shown in Figure 15. The trench diagram is not to scale and only shows the relative locations of each piezometer.

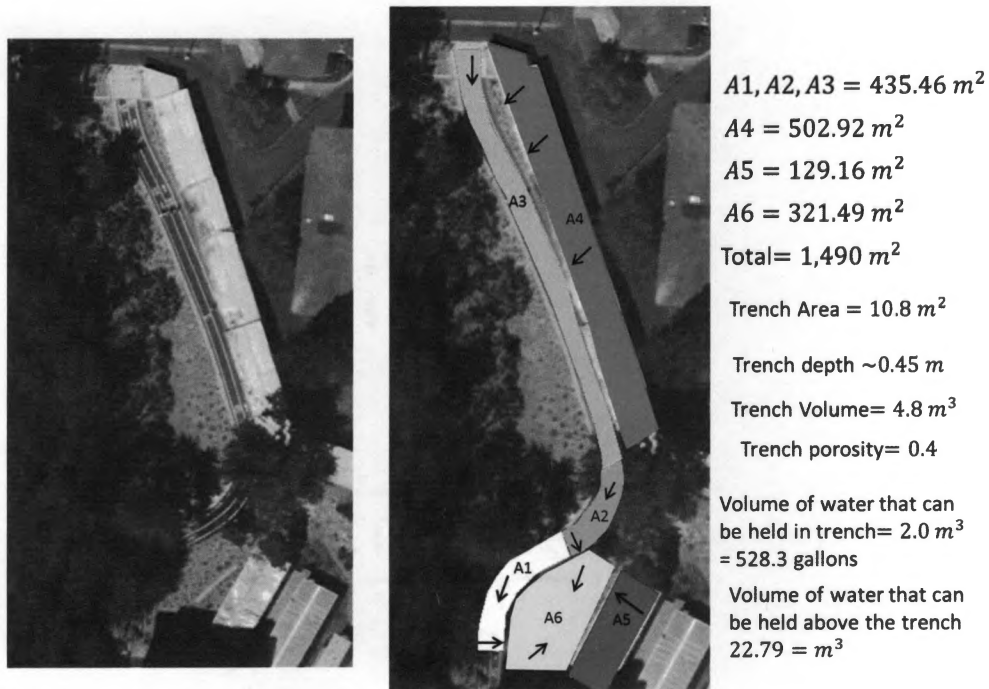


Figure 14: Maximum drainage area for the LID infiltration pond.

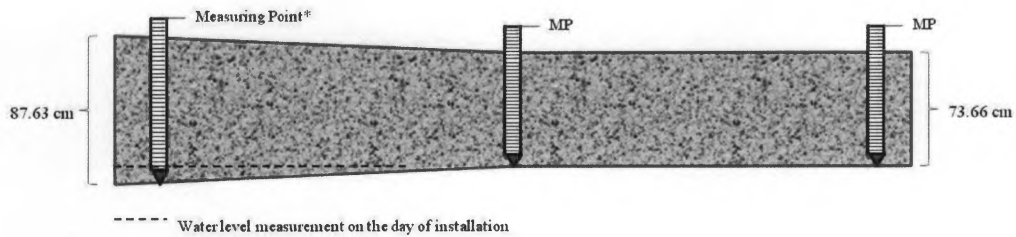


Figure 15: Cross-section of the infiltration trench and the three piezometers with pressure transducers

11.2 LID Stormwater Capture Capacity

11.2.1 Infiltration

Infiltration beneath the trench was analyzed using in-situ water level data in the gravel trench and the Green and Ampt Equation shown by Equations 1-4 below [Green and Ampt, 1911].

$$t_p = \frac{K_s * |\psi_f| * (\theta_s - \theta_r)}{w * (w - K_h)} \quad [1]$$

Where t_p is the time of ponding [T], K_s is the saturated hydraulic conductivity [L L⁻¹], ψ_f is the matric potential at field capacity [L] is solved using Equation 2 below, θ_s is the saturated water content, θ_r is the residual field content, w is the water input rate [L T⁻¹], and K_h is the unsaturated hydraulic conductivity [L T⁻¹],

$$|\psi_f| = \frac{2b+3}{2b+6} * |\psi_{ae}| \quad [2]$$

where b is the soil specific parameter (unitless), ψ_{ae} is the air-entry pressure head [L] obtained from the moisture retention curve [Dingman, 2002]. Once the time of ponding is calculated using Equation 1 and 2, Equations 3 and 4 are solved simultaneously for various inputs of $F(t)$, with $F(t)$ also used as an initial value for the cumulative infiltration.

$$f(t) = K_h * \left[1 + \frac{|\psi_f| * (\theta_s - \theta_r)}{F(t)} \right] \quad [3]$$

$$t = \frac{F(t) - F(t_p)}{K_h} + \left[\frac{|\psi_f| * (\theta_s - \theta_r)}{K_h} \right] * \ln \left[\frac{F(t_p) + |\psi_f| * (\theta_s - \theta_r)}{F(t) + |\psi_f| * (\theta_s - \theta_r)} \right] + t_p \quad [4]$$

where $f(t)$ is the instantaneous infiltration rate [$L T^{-1}$], and $F(t)$ is the cumulative infiltration [L], and $F(t_p)$ is the cumulative infiltration [L]. The Green and Ampt equation for infiltration was only used for calculating infiltration values for the water-budget when the system was no longer under ponded conditions, which rarely occurred. This is because during ponded conditions, the infiltration rate is equal to the saturated hydraulic conductivity. Infiltration rate and cumulative infiltration are shown in Figure 16.

The sources of infiltration beneath the trench include direct precipitation and irrigation, surface runoff from precipitation and irrigation, and roof/pavement runoff. Precipitation and irrigation contribute to infiltration at the irrigated lawn site until ponding occurs and excess water becomes runoff. There is no surface runoff to the lawn site.

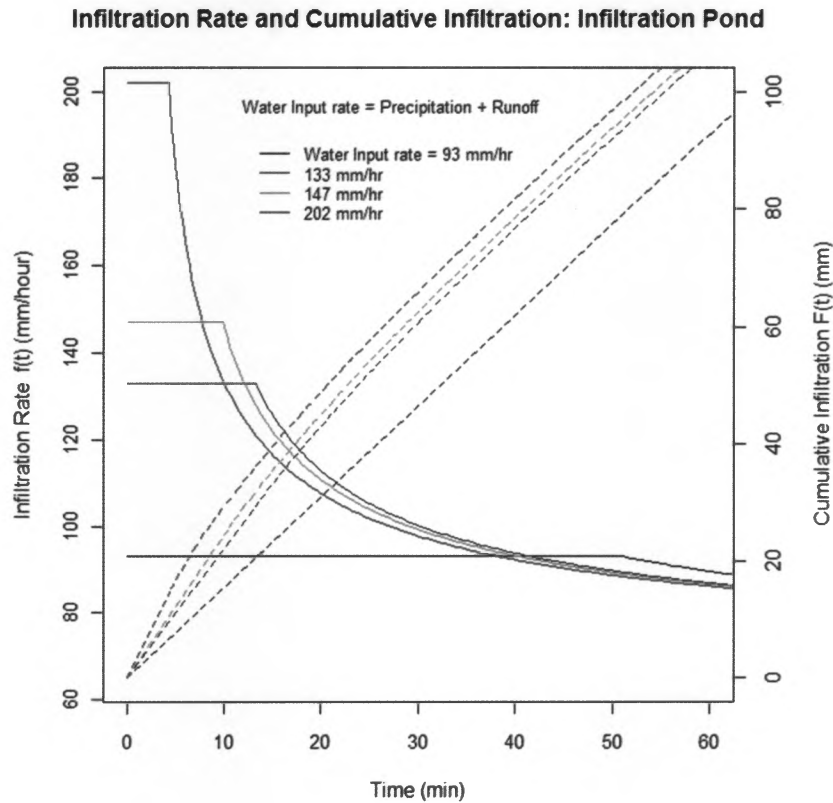


Figure 16: Infiltration rates and cumulative infiltration for the LID infiltration pond under different water input scenarios.

11.2.2 Runoff

Runoff was calculated for the infiltration trench and surrounding garden using the curve number and runoff approach as described in the TR-55 report [Natural Resources Conservation Service, 1986]. The maximum area of drainage is shown in Figure 14, however the effective area of drainage was about 1/3 the total hypothesized area of drainage. The effective area was defined as the area

actually contributing water volumes to the trench site which is much less than the maximum drainage area available. This area was calculated using the water volumes for one precipitation event and provides a large source of uncertainty to the volume estimates.

11.3 Methods for estimating recharge

Recharge is a subsurface hydrologic process where infiltrated water reaches the water table and is a function of the local climate. Rates of recharge are the vertical and volumetric flux of water across the water table and expressed as volume per time (cubic millimeters per year) or more commonly as length per time (such as millimeters per year). Intense precipitation events can immediately affect recharge in aquifers having shallow water tables, such as in humid regions, whereas in arid and semi-arid regions, recharge generally has a slower, less-dramatic response to precipitation events in these aquifers with deep water tables [Alley *et al.*, 2002]. In some desert regions, pore-water in the vadose zone is estimated to have infiltrated 120,000 years ago and has not yet reached the water table [Alley *et al.*, 2002].

Groundwater recharge in urban areas is more complex and spatially heterogeneous than recharge in rural environments. Buildings, roads, subsurface infrastructure, and drainage systems transport a large volume of water through the built environment and it is estimated that leaks from these systems contribute a

large portion the recharge to urban aquifers [*Lerner, 2002*]. *Lerner* [1990] proposed that recharge is greater in urban areas because of these subsurface features that direct water past the root zone and contribute to the water table, also citing the lack of data quantifying the water budget from urban features.

Recharge is important to estimate in urban areas for determining the transport and fate of contaminants in the groundwater system. Relatively short travel times may enhance preferential flow of surface contaminants and enhance groundwater susceptibility to contamination, whereas relatively long travel times may promote contaminant degradation and reduce groundwater susceptibility to contamination [*Laws et al., 2011*]. Roof runoff, managed low-impact development recharge approaches, and subsurface leakage can enhance preferential flow and also introduce contaminants into the subsurface placing high importance on understanding recharge mechanisms for managed low-impact development approaches [*SFPUC, 2010; Vialle et al., 2011*].

Recharge can be defined as diffuse or localized [*Lerner, 2002*]. Diffuse recharge refers to spatially homogeneous and widespread movement of water from land surface through the vadose zone, whereas localized recharge refers to movement from the land surface that is spatially heterogeneous and contributes to preferential flow in a specific area, for example under lakes, streams, and topographic lows [*Alley et al., 2002*]. In humid, arid, and semi-arid settings, most infiltration does not become recharge, and instead is eventually returned to the

global hydrologic cycle through evapo-transpiration [Alley *et al.*, 2002]. The ratio of infiltration to recharge is important for estimating water levels especially in urbanized environments where most precipitation becomes runoff and infiltration is spatially heterogeneous from both diffuse and localized recharge paths.

Factors that influence the rate and quantity of recharge include soil type, terrain, vegetation, precipitation, depth to the saturated zone, and urban diversion structures. Recharge can be difficult to quantify without direct *in-situ* measurements. Precipitation, stream interactions (losing streams), temperature, wind speed, solar radiation, evaporation, topography, vegetative cover, lithologic units, structural geology, and human influences are just a few of the variables that must be quantified to create an accurate water budget [UNESCO, 2008].

An example of a direct recharge measurement method is described by Gurdak *et al.* [2007]. In a study of the High Plains aquifer in the central United States, Gurdak *et al.* [2007] used well data and vadose zone instruments and found large water fluxes and strong lag correlations with climate variations during ENSO and PDO [Gurdak *et al.*, 2007]. Measurements taken at each site included processes and rates of water movement, and the storage and transit time of chemicals. Measurements such as these provide information about the vadose zone and the aquifer and show that large recharge events may occur in response to interannual to multidecadal climate variability [Gurdak *et al.*, 2007]. A study in 1993 found that approximately 440 acre-ft of recharge occurs every year in the

Westside Basin Aquifer [Brown *et al.*, 1997]; however, responses in the vadose zone to LID approaches and to climate variations have not been documented generally or for the Westside Basin aquifer [Dietz, 2007; US EPA, 2000]. Direct *in-situ* measurements are needed to more precisely model potential changes to recharge beneath LID and to this aquifer.

Approximating the total volume of recharge to urban aquifers requires estimates for liquid flux between the land surface and the water table. Methods for measuring flux in the shallow subsurface include pan lysimeters [Parizek and Lane, 1970], tension lysimeters [Brye *et al.*, 1999], vadose zone flux meters [Gee *et al.*, 2002], and Darcian approaches [Hubbell *et al.*, 2004].

11.4 Darcy Method

Darcian approaches to estimating groundwater recharge are typical in most groundwater studies where soil properties and flux data are available [Allison *et al.*, 1994; Healy, 2010; Scanlon *et al.*, 2002]. The Darcy method has been applied in many different climatic regions. If used in the one-dimensional form, this method requires the use of matric potential measurements in the field, however in certain circumstances where the zones are uniform, a unit-head gradient is assumed, removing the necessity for *in-situ* measurements [Scanlon *et al.*, 2002b]. Hydraulic conductivity measurements are also required for using the Darcy approach, and these can typically be obtained by infiltrometer field

measurements, laboratory methods, or estimated using a pedo-transfer function and sediment textural distribution [Dingman, 2002].

11.5 Water Budget Method

In simplified form, recharge can be expressed as the change in storage term shown in Equation 7:

$$\text{Recharge} = \text{Infiltration} - \text{Evaporation} \quad [7]$$

Simplified water balance equations such as the one above, are not necessarily useful for large urban areas because the city-wide scale incorporates other factors such as leakage, irrigation, drainage, and runoff [Lerner, 2002]. Given that hourly and daily precipitation values were available, a water budget method was appropriate at both the LID infiltration trench site and the grass lawn site.

11.5.1 Irrigation Audit

Irrigation was measured manually at the conventional grass lawn site using the techniques described in *The Irrigation Association* (2010). Measuring cups were placed adjacent to, and in-between each sprinkler head (Figure 17). A 9-minute irrigation run was conducted and the resulting volumes were measured. Volumes were averaged and the resulting irrigation flow was calculated using Equation 9. Irrigation for the grass lawn was calculated at 3.12 cm/hour. Since

irrigation takes place three times per week, two times each day, for nine minutes during each session, this converts to 2.81 cm/week.

$$\text{Irrigation rate} = \frac{3.66 * V_{avg}}{t * A} \quad [9]$$

Where:

V_{avg} = average volume (mL)

t = testing run time (min)

A = cup throat area (in²)

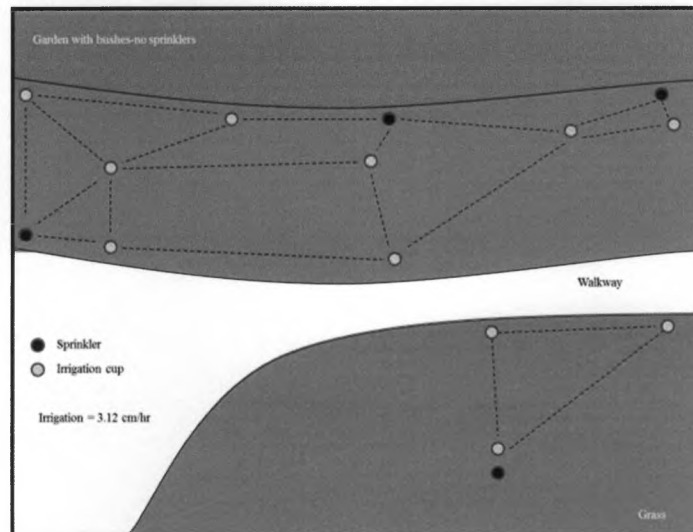


Figure 17: Location of the cups used for the irrigation audit.

11.6 Recharge Probability

11.6.1 Probability Density Function from an Exponential Distribution

Probabilities and probability densities were calculated from the Mission Dolores data summarized by day. The exponential probability density function (PDF) is given by Equation 10 [Helsel and Hirsch, 2002; Crawley, 2007]:

$$f(p) = \lambda e^{-\lambda p}, p \geq 0 \quad [10]$$

Where:

$\lambda=1/\mu$

μ =mean

p =precipitation values

Integrating the PDF provides the probability of that event occurring. The probability (Pr) that any rain event (P) will be greater than or equal to a rain event of interest (p), $Pr(P \geq p)$ is characterized by the cumulative density function CDF (integral of the PDF) shown by Equation 11 and the density frequency and PDF curve are shown in Figure 18. The density frequency is calculated by dividing the frequency of the data bin by the total number of occurrences:

$$Pr(P \geq p) = 1 - F(p) = 1 - \int_0^p \lambda e^{-\lambda P} dP, p \geq 0 \quad [11]$$

$$F(p) = 1 - e^{-\lambda p}, p > 0$$

$$Pr(P \geq p) = 1 - F(p) = e^{-\lambda p}, p > 0$$

The probability and the cumulative probabilities were calculated for various bins of precipitation including the rain events specified by the exceedence probability analysis for comparison. Once the probabilities were calculated, the

probability values were input into the curve number analysis for calculating precipitation that drains into the trench and garden and calculating the total likely volume of water that will drain into the system or overflow. Probability densities are a function of the frequency of the data and allow datasets to be compared independently of the number of observations. The probability is the area under the probability density curve and to the right, giving a value of probability that any rain event will be at that value or exceed that value.

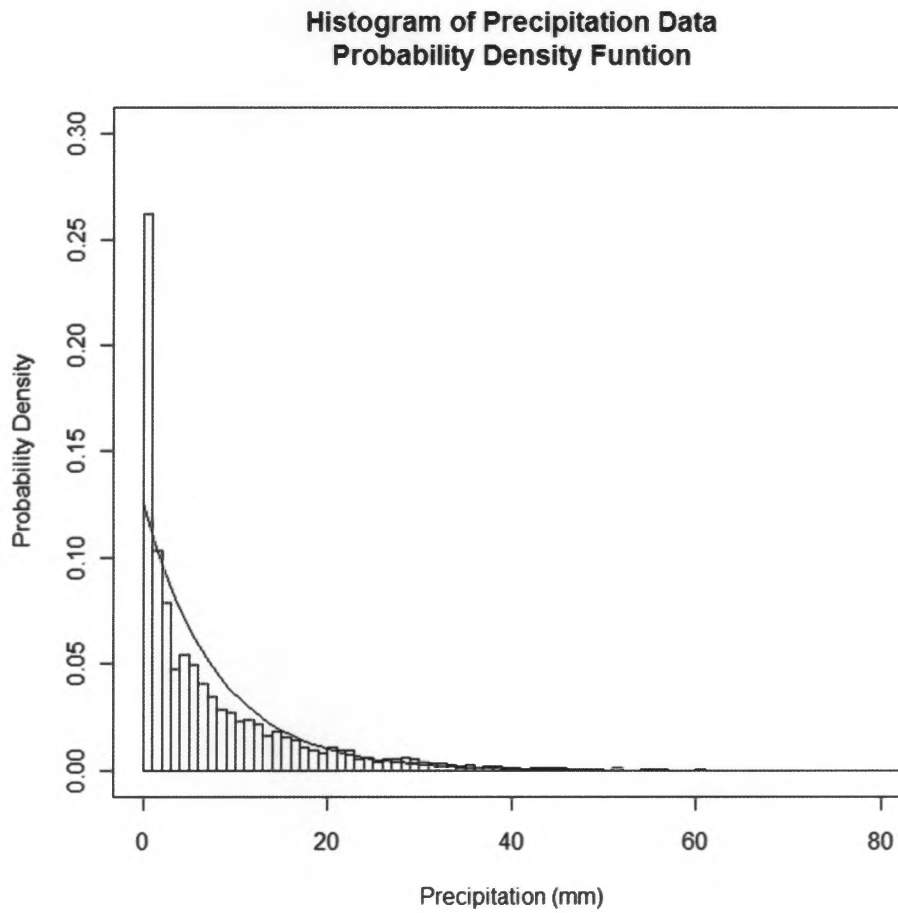


Figure 18: Exponential probability density function for the historical precipitation data.

11.6.2 Precipitation Exceedence Probability and Depth Duration Frequency Analysis

The exceedence probability that any particular rain event will occur is a measure of how often a particular rain event will occur during a specified time period. The probability that a rain event of a certain size will occur is a function

of the specific meteorological conditions of the area. The exceedence probability of 1-hour, 6-hour, and 24-hour rain events were calculated for 2-year, 5-year, 10-year, and 25-year timeframes to determine the probable return period of a specific rain event. This analysis was conducted using 3 steps: 1) creating depth-duration-frequency graphs, 2) ranking the data and calculating the exceedence probability and recurrence interval, and 3) plotting the data using a probability scale (Figure 16) [Dingman, 2002].

Depth-duration-frequency (DDF) analysis was initiated with hourly precipitation values from the Oceanside station. The purpose of this was to estimate the depths of rainfalls of durations of 1, 6, and 24 hours with return periods of 2, 5, 10, and 25 years. Data were ordered and ranked for the 1, 6, and 24-hr intervals and the exceedence probability was calculated using Equations 10 and 11 and displayed on a probability graph to determine the rainfall amounts for the return period of interest (Figure 19). The capacity for the LID infiltration trench to overflow was analyzed for a 2-yr 24-hr rain event, a 5-yr 24-hr rain event, a 10-yr 24-hr rain event, a 25-yr 24-hr rain event, and a 50-yr 24-hr rain event.

Recharge probability for the yearly probability distribution of rain events was calculated for each of the seven different precipitation scenarios. This is accomplished by taking the probability density function of the specific yearly rain distribution for that scenario and applying the probability density coefficient to

the runoff value. The runoff entering the irrigation trench, within the 2 m³ capacity of the trench becomes infiltration. From the water budget equation, the percentage of recharge from a specific quantity of infiltration was calculated and this percentage then applied to the total yearly infiltration probability values to calculate a yearly recharge probability value.

Exceedence probability of 1-hour, 6-hour, and 24-hour rain events

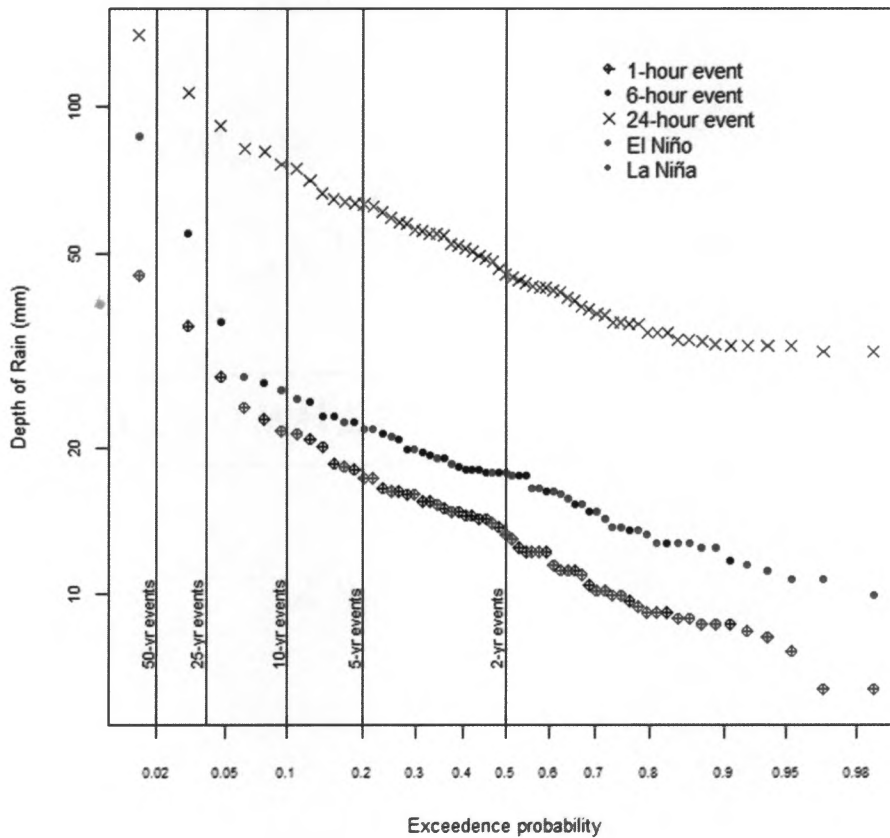


Figure 19: Exceedence probability of 2, 5, 10, 25, and 50 year 1-hr, 6-hr, and 24-hr storms. ENSO events are shown in blue and red.

11.7 Modeling Recharge

Vadose zone models that have been calibrated with subsurface properties provide a method for comparing observed recharge with modeled recharge, and if they agree, the vadose zone model can be used to simulate future recharge. An

important component of modeling recharge rates and analyzing water movement through the vadose zone is the collection of field parameters as input to vadose zone models. Collection of soil cores and measurement of field infiltration can provide parameters for creating water retention functions which are used for predicting the water content at various depths throughout the soil column using the Retention Curve program (RETC) [*van Genuchten et al.*, 1991]. Water retention functions relate pore-water content to soil matric potential, the function of which provides fitting-parameters that are further used in the Hydrus program [*Simunek et al.*, 2008; *PC-Progress*, 2011] for modeling water movement and for predicting the unsaturated hydraulic conductivity for the soil column. Hydrus is a computer program that numerically solves the Richards equation [*Richards*, 1931] shown by Equation 12 for saturated/unsaturated water flow and Fickian-based advection dispersion equations for heat and solute transport [*Simunek et al.*, 2008; *Dingman*, 2002].

$$\frac{\partial \theta}{\partial t} = \frac{\partial}{\partial z} \left[K(\theta) * \frac{\partial \psi(\theta)}{\partial z} \right] - \frac{\partial K(\theta)}{\partial z} \quad [12]$$

Where:

$\delta\theta/\delta t$ = the change in water content with respect to time (T^{-1})

$K(\theta)$ = unsaturated hydraulic conductivity (L/T)

$\delta\psi(\theta)/\delta t$ = the change in matric potential as a function of water content with respect to depth (L/T)

$\delta K(\theta)/\delta t$ = the change in hydraulic conductivity (L/T) as a function of water content with respect to depth (L/T)

Typically, the one dimensional and three dimensional Richards Equation must be solved with boundary conditions, initial conditions, and a few known parameters—mainly water content and matric potential. The ψ - θ and the $K(\theta)$ - θ relations are crucial determinants of unsaturated flow and must be characterized to solve the Richards Equation.

11.7.1 Water content-matric potential relation

Brooks and Corey (1964), Campbell (1974), and van Genuchten (1980) have proposed different versions of the ψ - θ and the $K(\theta)$ - θ relations [Brooks and Corey, 1964; Campbell, 1974; Van Genuchten, 1980]. For purposes of this study, the Van Genuchten equations were used to best utilize the RETC and Hydrus-3D programs [PC-Progress, 2011]. The van Genuchten equations are shown below in Equation 13 and Equation 14.

$$\theta(h) = (\theta_s - \theta_r)[1 + (\alpha h)^n]^{-m} + \theta_r \quad [13]$$

Where:

$\theta(h)$ = volumetric water content as a function of matric potential

θ_s = saturated water content

θ_r = residual water content

α = van Genuchten parameter

n = van Genuchten parameter

$m = 1 - 1/n$ van Genuchten parameter

$$K_r(h) = \frac{\{1 - (\alpha h)^{n-1} [1 + (\alpha h)^n]^{-m}\}^2}{[1 + (\alpha h)^n]^{m/2}} \quad [14]$$

$$K(h) = K_s * K_r(h)$$

Where:

$K_r(h)$ = the relative hydraulic conductivity as a function of matric potential

$K(h)$ = unsaturated hydraulic conductivity

K_s = saturated hydraulic conductivity

Knowledge of the soil textures and bulk density are necessary inputs to the RETC code for predicting the van Genuchten parameters. The RETC code then build a moisture retention curve and calculates α , n , m , θ_r , θ_s , and K_s . The van Genuchten parameters are then used to specify the specific soil hydraulic properties in Hydrus-3D.

11.8 Laboratory Analysis

For each site, and each lithologic unit, soil samples were collected for analyzing soil grain-size, and for building water-retention curves. Water-retention curves were built from each soil core using the WP4 Water Potentiometer. The WP4 measures the matric-potential in the soil at different values of water content. Different soil types have varied properties related to water content and movement, and predicting recharge in Hydrus-2D requires the water-retention curves for predicting unsaturated and saturated hydraulic conductivities [*Decagon Devices*, 2009].

11.9 RETC

Water retention curves are necessary for predicting the van Genuchten fitting parameters necessary for analyzing water movement in the unsaturated zone. Because the WP4 measure matric-potential only measure matric potential in the dry end of the spectrum, it was necessary to use a dual phase process in obtaining the final van Genuchten parameters and for obtaining a reasonable fit in the wet region of the water content spectrum. First data were entered into RETC [*van Genuchten et al.*, 1991] as-is and the program allowed to find the best fit with the available data. Fitted curves were then compared with RETC generic curves for different soil types based on the soil texture analysis to find the best match. Curves produced from RETC are shown in Figure 20.

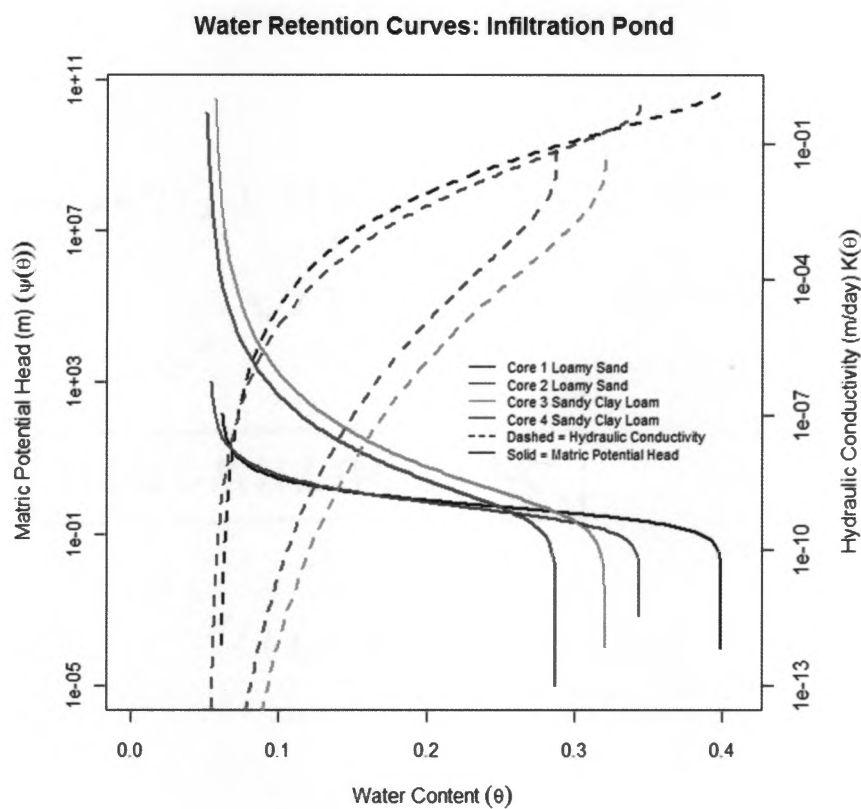


Figure 20: Water retention curves for the 4 soil samples taken at the infiltration LID site.

11.10 References

- Alley, W. M., R. W. Healy, J. W. LaBaugh, and T. E. Reilly (2002), Flow and Storage in Groundwater Systems, *Science*, 296(5575), 1985–1990, doi:10.1126/science.1067123.
- Allison, G. B., G. W. Gee, and S. W. Tyler (1994), Vadose-zone techniques for estimating groundwater recharge in arid and semiarid regions, *Soil Science Society of America Journal*, 58(1), 6–6.

- Brooks, R. H., and A. T. Corey (1964), *Hydraulic properties of porous media*, Colorado State University Hydrology Paper 3, Colorado State University, Fort Collins, CO.
- Brown, M., T. Pezetti, F. Carlson, and L. Dumas (1997), *Technical Memorandum No. 18 Westside Basin Groundwater Model*, Technical Memorandum #18, San Francisco Public Utilities Commission.
- Bruce, B., D. Allen, H. Chaves, G. Grant, G. O. Essink, H. Kooi, I. White, J. Gurdak, J. Famiglietti, and J. L. Martin-Bordes (2008), Groundwater Resources Assessment under the Pressures of Humanity and Climate Changes, *United Nations Educational, Scientific and Cultural Organization (UNESCO)*, 32.
- Brye, K. R., J. M. Norman, L. G. Bundy, and S. T. Gower (1999), An equilibrium tension lysimeter for measuring drainage through soil, *Soil Science Society of America journal*, 63(3), 536.
- Campbell, G. S. (1974), A simple method for determining unsaturated hydraulic conductivity from moisture retention data, *Soil Science*, 117, 311–314.
- Crawley, M. J. (2007), *The R Book*, John Wiley, & Sons, Ltd, Chichester, Imperial College London at Silwood Park, UK.
- Decagon Devices (2009), *Generating a Soil Moisture Characteristic Using the WP4*. [online] Available from: http://www.decagon.com/pdfs/app_notes/GeneratingaSoilMoistureCharacteristicUsin.pdf
- Dietz, M. E. (2007), Low Impact Development Practices: A Review of Current Research and Recommendations for Future Directions, *Water, Air, and Soil Pollution*, 186(1-4), 351–363, doi:10.1007/s11270-007-9484-z.
- Dingman, S. L. (2002), *Physical Hydrology*, Prentice-Hall, Inc., University of New Hampshire.
- Gee, G. W., A. L. Ward, T. G. Caldwell, and J. C. Ritter (2002), A vadose zone water fluxmeter with divergence control, *Water Resources Research*, 38(8), doi:10.1029/2001WR000816.

- van Genuchten, M. T. (1980), A closed-form equation for predicting the hydraulic conductivity of unsaturated soils., *Soil Science Society of America Journal*, 44, 892–898.
- van Genuchten, M. T., F. J. Leij, and S. R. Yates (1991), *The RETC Code for Quantifying the Hydraulic Functions of Unsaturated Soils*, U.S. Salinity Laboratory, USDA, ARS, Riverside, California.
- Green, W. H., and G. A. Ampt (1911), Studies on Soil Physics: The flow of air and water through soils, *The Journal of Agricultural Science*, 4(01), 1–24, doi:10.1017/S0021859600001441.
- Gurdak, J. J., R. T. Hanson, P. B. McMahon, B. W. Bruce, J. E. McCray, G. D. Thyne, and R. C. Reedy (2007), Climate Variability Controls on Unsaturated Water and Chemical Movement, High Plains Aquifer, USA, *Vadose Zone Journal*, 6(3), 533–547, doi:10.2136/vzj2006.0087.
- Healy, R. W. (2010), *Estimating Groundwater Recharge*, Cambridge University Press.
- Helsel, D. R., and R. M. Hirsch (2002), *Statistical Methods in Water Resources*, Techniques of Water-Resources Investigations Book 4, U.S. Geological Survey. [online] Available from: <http://pubs.usgs.gov/twri/twri4a3/>
- Hubbell, J. M., M. J. Nicholl, J. B. Sisson, and D. L. McElroy (2004), Application of a Darcian Approach to Estimate Liquid Flux in a Deep Vadose Zone, *Vadose Zone Journal*, 3(2), 560–569, doi:10.2113/3.2.560.
- Laws, B. V., E. R. V. Dickenson, T. A. Johnson, S. A. Snyder, and J. E. Drewes (2011), Attenuation of contaminants of emerging concern during surface-spreading aquifer recharge, *Science of The Total Environment*, 409(6), 1087–1094, doi:10.1016/j.scitotenv.2010.11.021.
- Lerner, D. (2002), Identifying and quantifying urban recharge: a review, *Hydrogeology Journal*, 10(1), 143–152, doi:10.1007/s10040-001-0177-1.
- Lerner, D. N. (1990), Groundwater recharge in urban areas, *Atmospheric Environment. Part B. Urban Atmosphere*, 24(1), 29–33, doi:10.1016/0957-1272(90)90006-G.

- Natural Resources Conservation Service (1986), *Urban Hydrology for Small Watersheds*, Technical Manual, United States Department of Agriculture-Conservation Engineering Division.
- Parizek, R. R., and B. E. Lane (1970), Soil-water sampling using pan and deep pressure-vacuum lysimeters, *Journal of Hydrology*, 11(1), 1–21, doi:10.1016/0022-1694(70)90111-3.
- PC-Progress (2011), PC-PROGRESS - Homepage, *PC-Progress Engineering Software Developer*. [online] Available from: <http://www.pc-progress.com/en/Default.aspx> (Accessed 13 January 2012)
- Richards, L. . (1931), Capillary conduction of liquids in porous mediums, *Physics*, 1, 318–333.
- Scanlon, B. R., R. W. Healy, and P. G. Cook (2002), Choosing appropriate techniques for quantifying groundwater recharge, *Hydrogeology Journal*, 10, 18–39.
- SFPUC (2010), SFWATER.ORG : Low Impact Design, [online] Available from: <http://sfwater.org/index.aspx?page=237> (Accessed 2 May 2011)
- Simunek, J., M. T. van Genuchten, and M. Sejna (2008), Development and Applications of the HYDRUS and STANMOD Software Packages and Related Codes, *Vadose Zone Journal*, 7(2), 587–600, doi:10.2136/vzj2007.0077.
- The Irrigation Association (2010), Landscape Irrigation Auditor,
- US EPA (2000), *Low impact development (LID), a literature review.*, United States Environmental Protection Agency.
- Vialle, C., C. Sablayrolles, M. Lovera, S. Jacob, M.-C. Huau, and M. Montrejaud-Vignoles (2011), Monitoring Of Water Quality From Roof Runoff: Interpretation Using Multivariate Analysis, *Water Research*, doi:10.1016/j.watres.2011.04.029.